Geophys. J. Int. (1990) **103**, 377–401

Observations on earthquake stress axes and seismic morphology of deep slabs

Hua-wei Zhou*
Seismological Laboratory, California Institute of Technology, Pasadena, CA 91125, USA

Accepted 1990 May 24. Received 1990 May 24; in original form 1989 April 18

SUMMARY

Focal mechanism solutions from centroid-moment tensor (CMT) and other studies in the NW Pacific and Tonga–Kermadec regions are analysed in association with velocity images from tomographic inversions. Deep compression axes and fast velocity slab anomalies are usually in consistent alignment, even when the slab is contorted or flattened. The down-dip direction for each event is given based on slab geometry interpreted from velocity anomalies and seismicity. The well-known pattern of tension to compression down-dip stress by Isacks & Molnar is seen and fitted with a tangent curve, which gives the location of the neutral down-dip stress zone (NDSZ). An abnormal pattern of NDSZ exists beneath major junctions of the arcs. The NDSZ is generally in the depth range of 100–250 km in the central parts of the arcs, while it is deeper in the Mariana region. The depth seems to depend on the dip and topology of the slab, but the NDSZ probably starts at more or less the same subducted length along the slab.

Key words: focal mechanisms, seismic tomography, stress, subducted slab.

INTRODUCTION

Since the birth of the plate tectonics the nature of the descending oceanic lithospheric slab in subduction zones has been an important issue due to its bearing on models of mantle convection and the chemical evolution of the Earth (Isacks, Oliver & Sykes 1968; Toksöz *et al.* 1973; Richter 1979; Hager, O'Connell & Raefsky 1983). Two important aspects about the slab are its seismic morphology and state of stress. Our knowledge about the morphology of the slab has relied primarily on the distribution of Wadati–Benioff zone earthquakes and seismic high-velocity, low-attenuation slab anomalies. These anomalies, which are interpreted as being primarily due to cold subducting lithosphere (e.g., Toksöz *et al.* 1971), have been observed beneath Japan and other arcs to depths of at least several hundred kilometres (e.g., Utsu 1971; Hirahara 1981). Slab-like fast anomalies in the upper mantle depth range are evident in recent 3-D tomographic inversions (e.g., Zhou & Clayton 1987, 1989; Kamiya, Miyatake & Hirahara 1988).

The state of stress in slabs is inferred primarily from stress axes of focal mechanism solutions for mantle earthquakes. Analyses by Isacks *et al.* (Isacks *et al.* 1968; Isacks, Sykes & Oliver 1969) and Isacks & Molnar (1969) suggested that earthquakes deeper than about 70 km occur within the descending lithosphere in response to stresses in the slabs. The primary support for their suggestion is that the down-dip direction, the local direction of subduction in a slab, is usually parallel with the compressional or tensional stress axes. In examining the relationship of earthquake stress axes to the orientation of Wadati–Benioff zones (in 2-D), Isacks & Molnar (1971) found consistent down-dip compression in the slabs below about 300 km depth, and down-dip tension or mixed stress at depths shallower than about 300 km. Actually, about half the focal mechanisms between 200 and 300 km indicate down-dip compression, and most of the mechanisms below 215 km are compressional (Anderson 1979). Recent global reviews of intermediate-depth earthquake mechanisms in association with subduction process can be found in Astiz, Lay & Kanamori (1988) and Lay *et al.* (1989).

The research described here extends the analysis of earthquake stress axes in subduction zones into 3-D to explore the variation of state of stress in slabs along their strike and the relationship between the stress axes and seismic morphology of the slabs. This analysis is facilitated by the availability of a large quantity of reliable focal mechanism solutions, dense seismicity and detailed tomographic velocity images around some major subduction zones. Compared to 10 years ago, an order of magnitude more earthquake source mechanisms is now available. This is due to the development (Kanamori & Given 1981; Dziewonski, Chou & Woodhouse 1981) and routine determination of moment tensor inversions using new digital data. Valuable products are the centroid-moment tensor

* New address: Department of Geosciences, University of Houston, Houston, TX 77204-5503, USA.

(CMT) solutions of medium to large magnitude events since 1977 by the Harvard group [Dziewonski *et al.* (1981), Dziewonski & Woodhouse (1983), Giardini (1984) and routinely published solutions in issues of *Physics of the Earth and Planetary Interiors* since 1983]. The available moment tensor solutions have been analysed previously in a global context (Vassiliou 1984; Apperson & Frohlich 1987), and interpreted with viscous fluid models of subducting slabs (Vassiliou & Hager 1988). These works confirmed down-dip compression in the slab at depths below 300 km.

This paper concentrates on two west Pacific regions: from Kuril via Japan to Mariana and from Tonga to Kermadec (Fig. 1). These include most of the subducting slabs in which earthquakes occur nearly continuously throughout the depth range of the upper mantle. The particularly dense earthquake mechanism solutions in these two regions allow mapping of the neutral down-dip stress zone (NDSZ) which, in general, divides the deep down-dip compression regime from the shallower down-dip tension stress regime. The relationship between earthquake stress axes and seismic morphology of deep slabs in 3-D furnishes new insight into the physical state of slabs.

DATA

Source mechanisms

The principal axes of a double-couple mechanism solution, which is the best representation of the radiation pattern of most earthquakes, are also principal stress axes if the fault plane is a plane of maximum shear. Following previous studies (e.g., Isacks *et al.* 1968) the compressional (P), tensional (T) and null (B) axes from the double-couple solutions are assumed to be coincident with the principal stress axes in the slab. As shown in earlier studies, the inferred stress axes tend to be parallel or perpendicular to the down-dip direction of subduction, thus justifying the above assumption, at least for events deeper than 70 km.

Most shallow earthquakes (<70 km) in subduction zones occur in response to either relative motions between lithospheric plates, or bending and faulting of the plates near trenches (e.g., Christensen & Ruff 1983, 1988). They are excluded from the analysis in this paper.

The focal mechanism data in this study consists of 776 solutions (see Table 1 in the Appendix) from published seismic first motion studies in the two west Pacific regions. Over 80 per cent of the solutions are from CMT catalogues of the Harvard group (events up to the end of September 1987). The compilation also includes events from the original collection of Isacks & Molnar (1971), and solution sets by Chandra (1971), Oike (1971), Stauder & Maulchin (1976), Sengupta & Tosköz, (1977), Billington (1978), Richter (1979), Fujita & Kanamori (1981) and Astiz *et al.* (1988). All solutions are generally well constrained. No attempt is made here to discard or modify any of the mechanism solutions. Although there are several dozen solutions for events which occurred before 1960, most of the data covers the time period from 1960 to 1987. The P- and T-axes from these mechanism solutions are plotted in stereo pairs for 3-D viewing (e.g., Fig. 2).

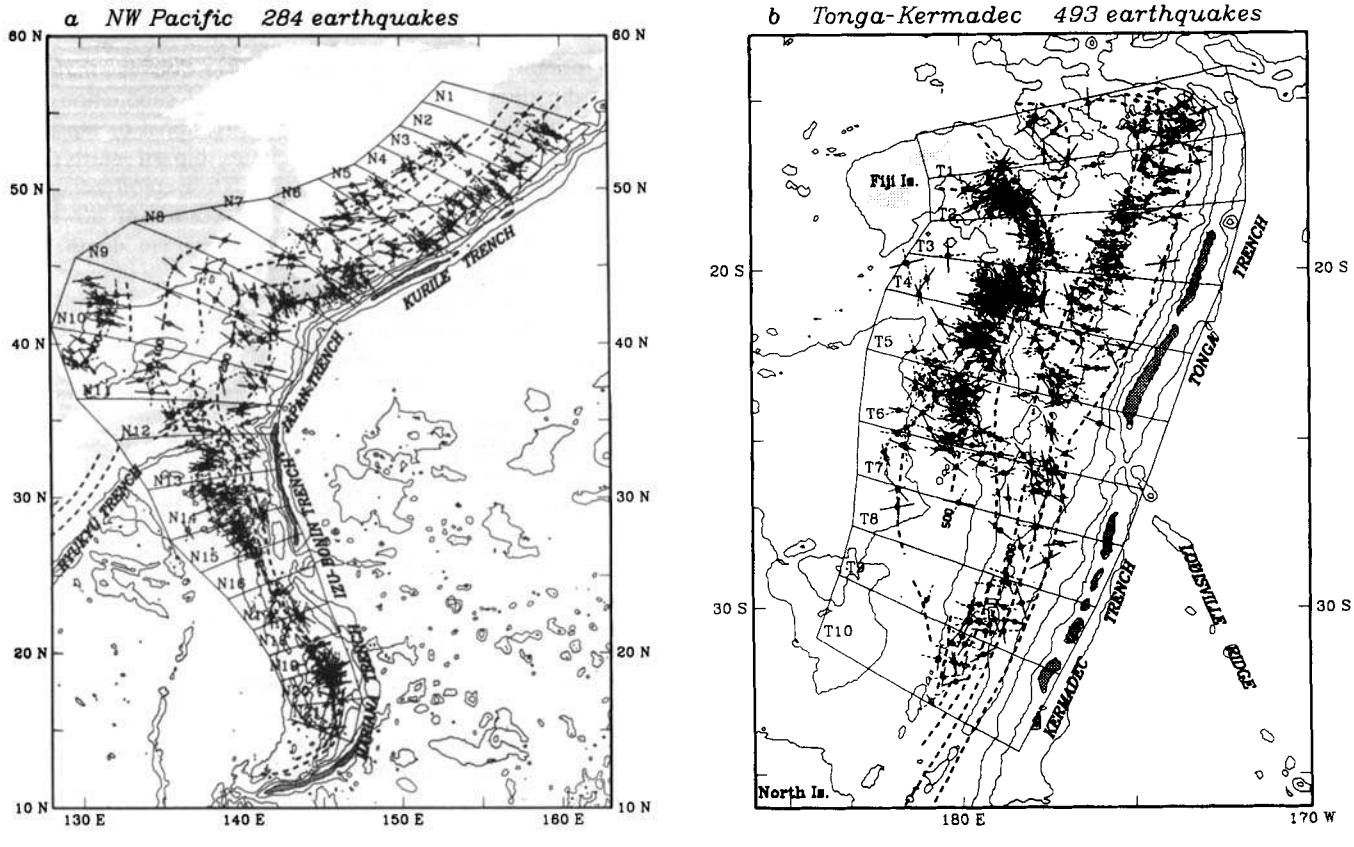

Figure 1. Regional maps: (a) NW Pacific; (b) Tonga–Kermadec. Heavy dashed lines contours deep seismicity at 100 km intervals, and light contour line shows 2 km isobath. Small circles denote earthquakes with available focal mechanisms, whose P- and T-axes are shown as solid and dashed bars, respectively, projected onto the map. The boxes indicate the locations of cross-sections normal to the strike of the slab.

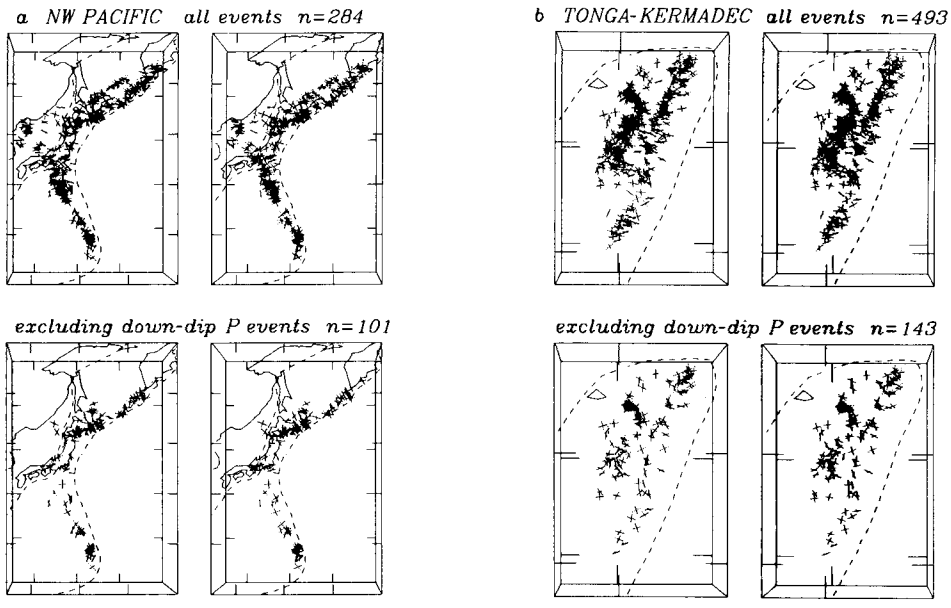

Figure 2. Stereo views of principal stress axes. (a) NW Pacific; (b) Tonga–Kermadec. There are two pairs of plots for each region; the top pair shows all mechanism solutions and the bottom pair excludes down-dip compressional events.

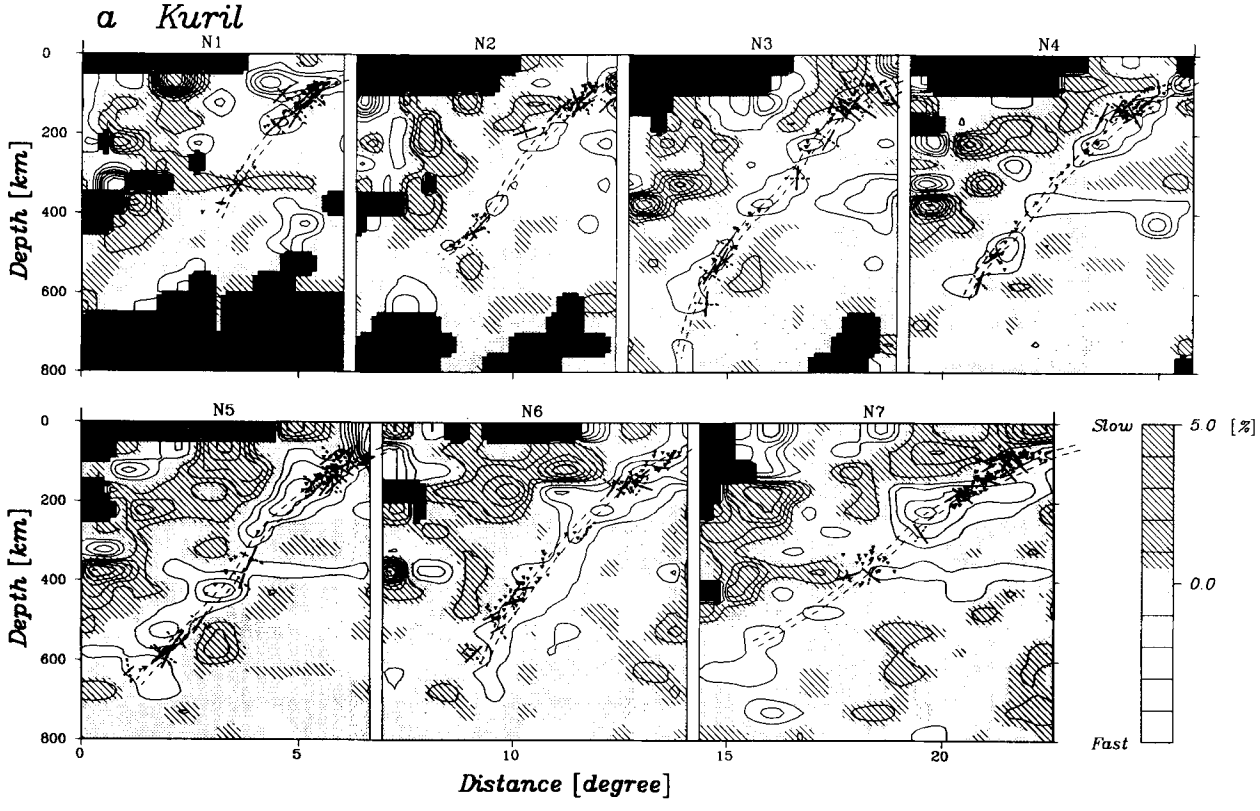

Figure 3. Cross-sections of *P*-wave velocity images with stress axes and interpreted slab trace. The locations of cross-sections are shown in Fig. 1. The velocities are stacked along the strike of the slab and contoured with 1 per cent intervals. White and cross-hatched areas are fast and slow velocities, respectively. Grey areas have less than a half per cent variation from the reference velocity; black denotes poorly sampled areas. *P*- and *T*-axes of available focal mechanism solutions are projected onto each panel. Other earthquake foci are shown with small open triangles. The double dashed lines display the slab trace interpreted from fast slab-like anomalies and the seismicity distribution.

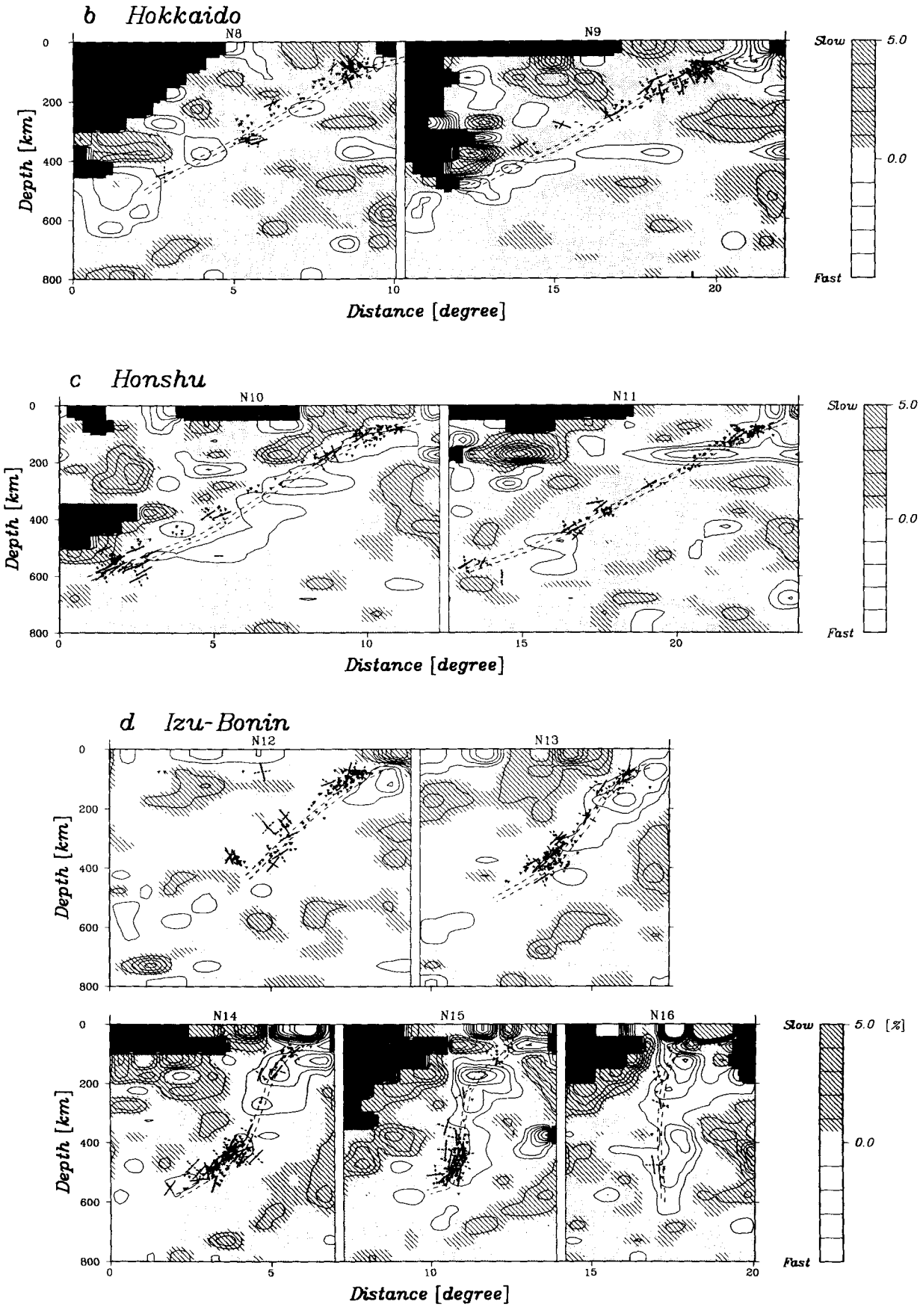

Figure 3. (*continued*)

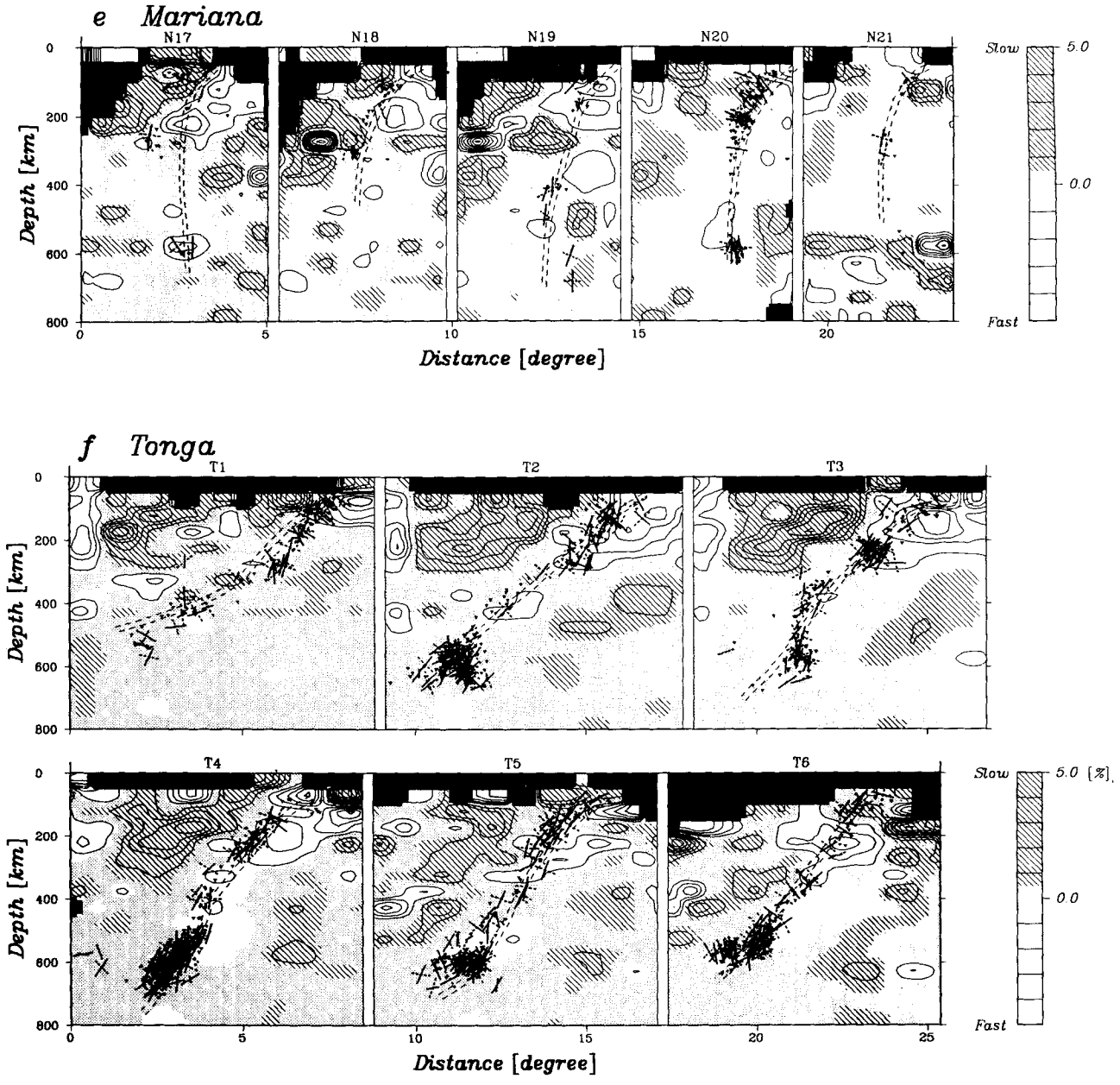

Figure 3. (*continued*)

Seismic velocity structures and seismicity

To facilitate the analysis of down-dip stress regime, we made a series of cross-sections normal to the strike of the slab, using the seismicity contours shown in Fig. 1. We then interpreted slab trace based on seismicity distribution and fast slab-like anomalies in the tomographically derived velocity structures in each cross-section.

Figure 3 displays the *P*-wave velocity images in these cross-sections, with earthquake foci, stress axes and interpreted slab trace. The velocity structures are from tomographic inversion studies for the two regions (Zhou & Clayton 1987, 1988) using earthquake traveltime data compiled by the International Seismologic Centre (ISC). The details about these tomographic investigation are discussed in Zhou (1988, 1990) and Zhou & Clayton (1990). Basically, the velocity structure in the NW Pacific is based on regional data, while teleseismic data is included for velocity inversion in the Tonga and Kermadec regions. The resolution cells of the images are roughly $100 \times 100 \times 50\,km^3$. Tests on resolution and noise for the inversion suggest that most patterns in these images are well resolved; however, anomalies near the edge of the covered region are noisier, and resolution for amplitude becomes poorer with depth.

To at least 700 km depth, subducted lithospheres have higher seismic velocity because they are about 800 °C cooler than the ambient mantle (e.g., Tosköz *et al.* 1973; Anderson 1987). This gives the basis for interpreting slab trace from slab-like velocity anomalies associated with the Wadati–Benioff zone. Indeed, the images in most slices of Fig. 3 show coherent fast slab-like anomalies around the

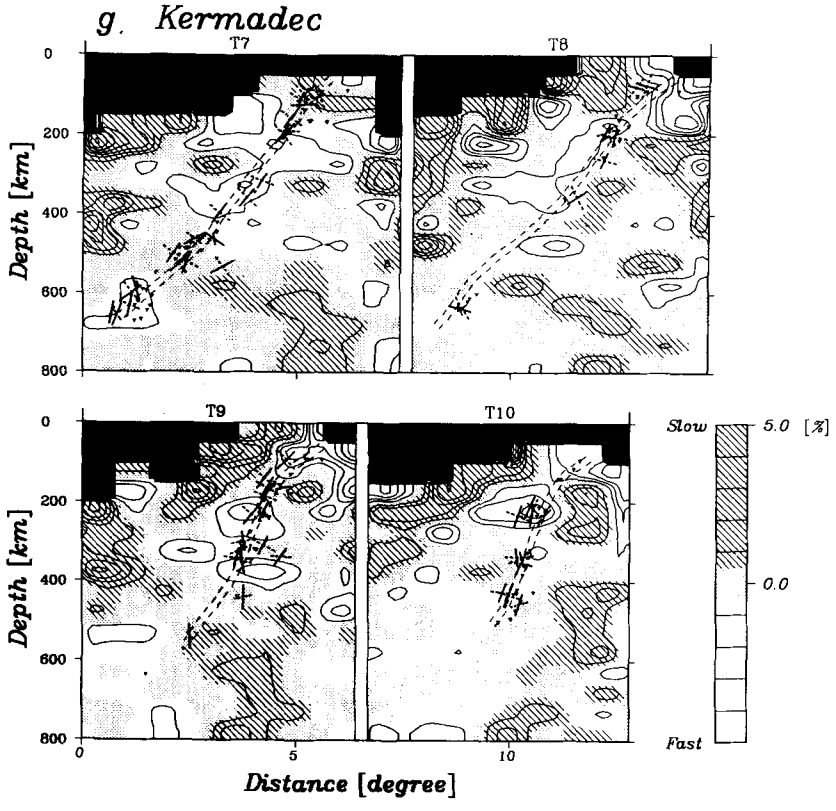

Figure 3. (*continued*)

Wadati–Benioff zones, even in places of sparse seismicity, surrounded by large slow anomalous patches which usually dominate the top 300 km depth range. In the lower part of the upper mantle the down-dip compression axes consistently follow the trend of fast velocity anomalies associated with Wadati–Benioff zones, even in cases where the anomalies are contorted or flattened to subhorizontal around the earthquake clusters at the bottom of the upper mantle beneath the Izu–Bonin arc (N13, N14 and N15) and the Tonga arc (T4, T5, T6 and T7). The down-dip compression pattern at depth therefore may be taken as an useful reference in inferring subducting slabs from seismic velocity structures.

The seismicity distribution is depicted using the ISC earthquake locations in the time period of 1964–1985. Earthquake Wadati–Benioff zones in most parts of the regions are continuous from the surface down to about 650 km. The dip of these zones, however, varies considerably, especially in the NW Pacific region (Fig. 2); it ranges from about 30° under Honshu to nearly vertical under the Mariana arc. In the down-dip direction, the Wadati–Benioff zone is relatively smooth in many places, but it is heavily contorted under the Izu–Bonin and Tonga arcs, and flattens to subhorizontal at its deepest extent. The contortion and flattening, perhaps unsurprisingly, produce some of the most distinguishable deep seismicity peaks at these places (Vassiliou & Hager 1988) right above abrupt cut-offs in seismic activity. This kind of contortion pattern in the Tonga region has been taken as evidence for major shear deformation and lateral displacement of the deep slab (Giardini & Woodhouse 1984, 1986).

METHOD

Determining down-dip direction and stress index

A down-dip direction is defined as the local direction of subduction in a slab (Isacks *et al.* 1968; Isacks & Molnar 1969). A similar term, 'in plate', has also been recommended (Fujita & Kanamori 1981). Nevertheless, the term 'down-dip' is well understood, and the key issue then is to find the local down-dip direction for each earthquake.

Figure 4 shows how we define the down-dip direction for each individual event. At each cross-section normal to the strike of the slab, a projection point of each event onto the slab trace is found. The down-dip direction for this event is then given by the azimuth of the slice θ_s and the plunge (dip) δ_s of the slab trace at the projection point. We then compute the angles between the down-dip direction and each of the three stress axes and denote them by η_T, η_B and η_P, respectively. In addition, we compute a quantity L, the subducted length along the slab to the event, measured from the slab trace at 50 km depth to the projection point.

To quantitatively describe the orientation of stress in the down-dip direction, we define a parameter κ, called down-dip stress index,

$$\kappa = (\cos \eta_P - \cos \eta_T) \sin \eta_B. \quad (1)$$

The stress index κ is dimensionless, with a value in the interval of $(-1, 1)$. It represents geometrically the projection difference between P- and T-axes on the down-dip direction in 3-D. κ equals -1, 0 or $+1$ when the T-, B- or P-axis, respectively, coincides with the down-dip direction (η_T, η_B or η_P equal to zero). Hence, the

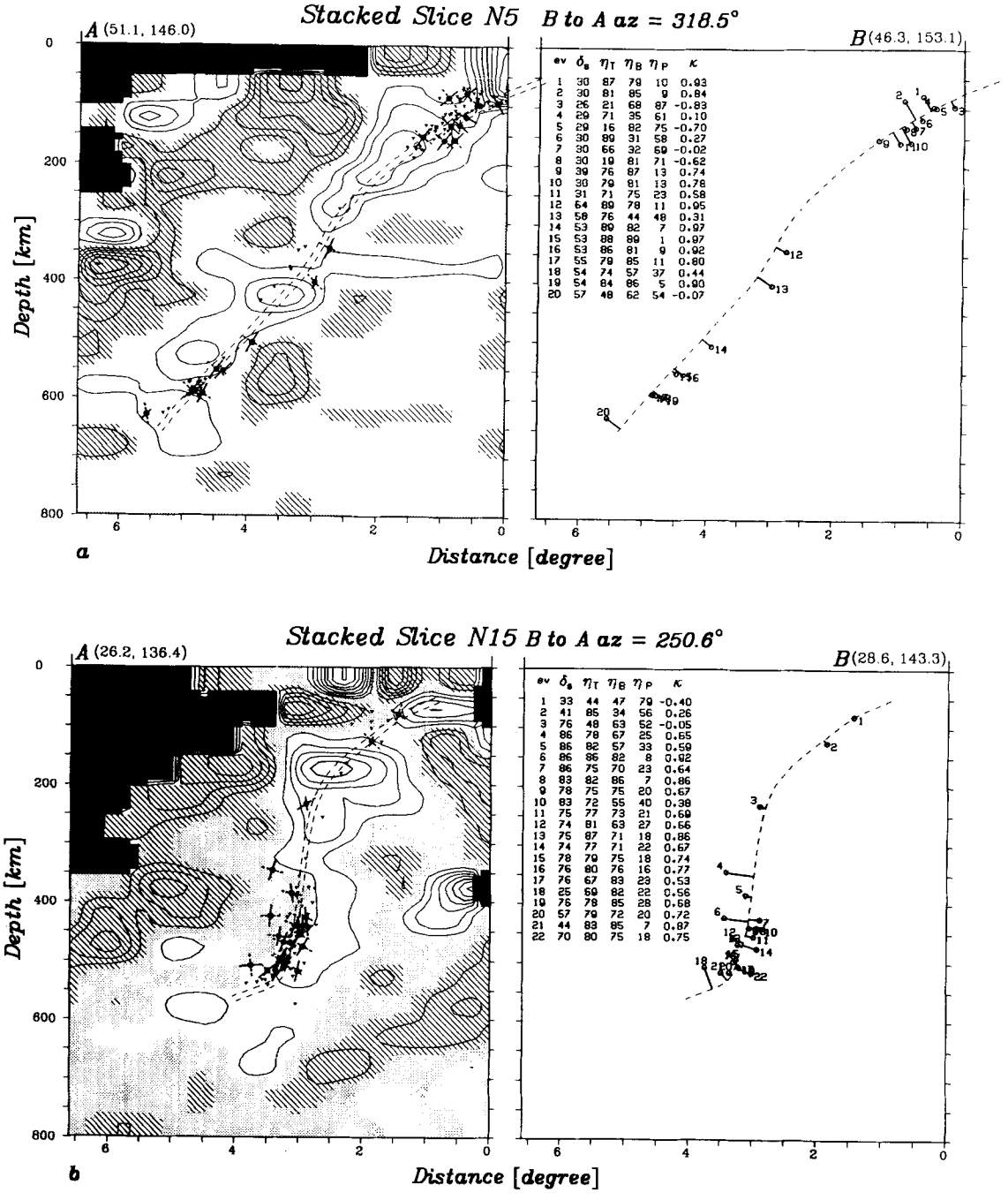

Figure 4. Examples of interpreting down-dip direction for each event: (a) slice N5; (b) slice N15. The left panel in each pair is the same as that in Fig. 3. The right one shows the projected location of each event on the slab trace (dashed curve). The down-dip direction for each event is given by the azimuth of the slice θ_s and the trace's plunge δ_s at the projection point. Consequently, the angles between the down-dip direction and three stress axes, η_T, η_B and η_P, and the down-dip stress index κ are obtained.

physical meaning of down-dip stress regime at each earthquake is quantified by the value of the stress index κ.

We should keep in mind that κ is computed based on the interpreted down-dip direction. Since the down-dip directions of all events in a slice are given with a constant azimuth θ_s, the down-dip direction and hence the κ value obtained could contain error, especially near the edge and bottom of the Wadati–Benioff zone where contortion of the slab may exist. Examples of extensive contortions are seen under the Tonga arc both in the deep Wadati–Benioff zones and in the seismic slab anomalies (Fig. 3f). Our analysis is therefore restricted to some first-order observations, such as that on the location of the NDSZ.

Table 1 in the Appendix lists stress axes of the 776 focal mechanism solutions, compiled with some slab-related parameters. Earthquakes in each slice are in a ascending order of the focal depths. δ denotes plunge and θ denotes azimuth. For instance, θ_s is the azimuth of each slice and $\bar{\delta}_s$

is the average slab plunge angle of all events deeper than 100 km in a slice.

Interpretation of the NDSZ locations

Since the κ values of all events are obtained we would like to find the location of the NDSZ, which is naturally near the place where κ is zero. To this goal, we plot the events in each slice according to their κ and L values in Fig. 5. Notice that the use of the subducted slab length L here is probably more physical than the focal depth. For example, in Fig. 4(a) event 2 is shallower than event 6 but the former has a larger L value than the latter.

Since the tension to compression relationship by Isacks & Molnar is clearly seen at most cross-sections, we attempt to fit the data in each κ–L plot with a tangent curve. We assume that the subducted slab length to the jth event, L_j, can be expressed as

$$L_j = L_0 + L_1 \tan(\kappa_j \times 90°), \quad (2)$$

where L_0 and L_1 are constant coefficients for each slice. L_0 is the value of L when κ equals to zero. L_1 is the length between two points on the L-axis where κ is at a half of its maximum magnitude. A smaller L_1 value thus indicates a more abrupt conversion from tension to compression and vice versa.

The non-linear form of equation (2) prevents us from a linear inversion. We hence fit the data in each slice by minimizing $\sum |d_j|$, where d_j is the distance from the jth data point to the fitting curve. The calculation of the distance involves multiplying the dimensionless κ value with a factor of 100 km. The choices of this factor as well as the tangent function form itself are purely subjective. All we attempt to do here, however, is to find a curve which uniquely fits the data with a small number of adjustable parameters, thus giving a computational base for interpreting the location of NDSZ. One could do the interpretation without any fitting function at all.

The best fitting tangent curve as well as our interpretation of the NDSZ for each slice are given in Fig. 5. The

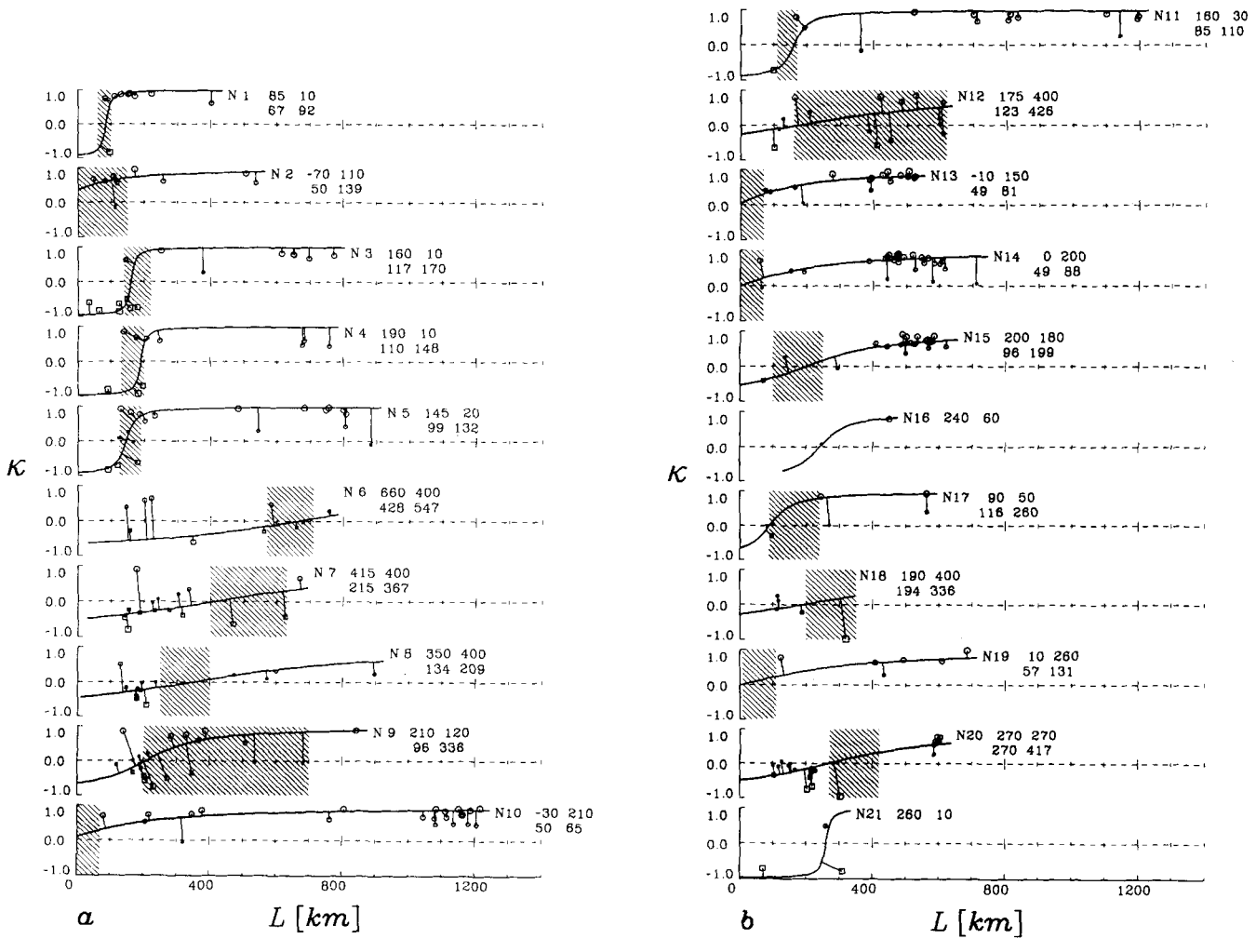

Figure 5. κ–L plots. (a) Slices N1–N10; (b) slices N11–N21; and (c) slices T1–T10. Circles and squares denote events of positive κ and negative κ values, respectively, and their size is proportional to the magnitude of κ. The heavy curve indicates the best fitting tangent curve, by

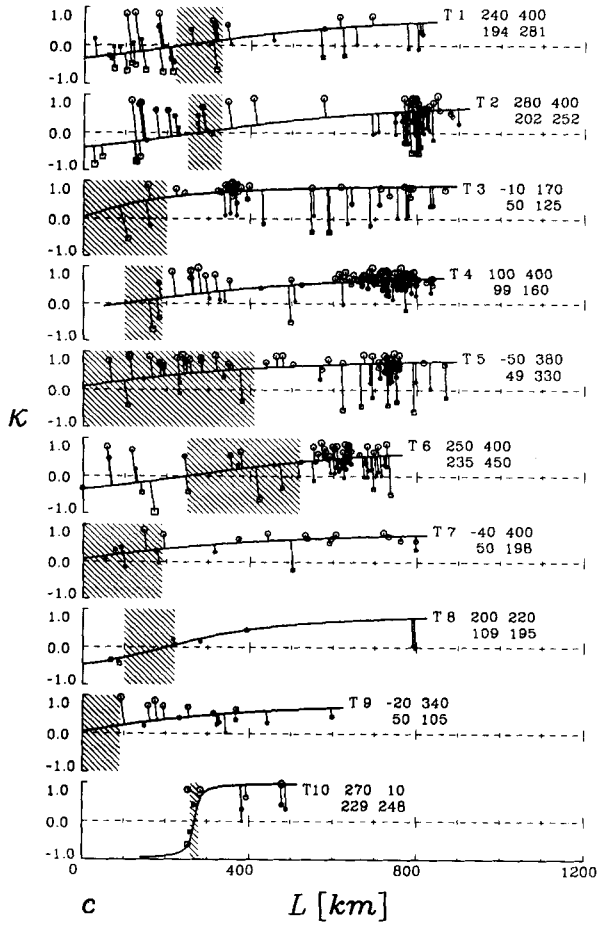

Figure 5. (*continued*)

interpretation is based on the locations of data points and the best fitting curve. No interpretation is given for slices N16 and N21 with insufficient number of data. The interpretation for some poorly fitted slices, such as N18, is with reference to the adjacent slices.

RESULTS

Down-dip stress in slabs

The down-dip tension to compression relationship by Isacks & Molnar is clearly seen at most cross-sections normal to the strike of the slab in this study. As shown in Fig. 3, deep compression axes and fast velocity slab anomalies are usually in consistent alignment, even when the slab is contorted or flattened. These motivate us to analyse the down-dip stress patterns in more detail.

The down-dip stress patterns in several of the slices in Fig. 5 appear to be abnormal, either by having a L range of the NDSZ abruptly larger than that of the adjacent slices (N6, N7, N9 and N12), or by possessing a number of very deep (or large L value) down-dip tensional events (T2, T5 and T6). These patterns, as discussed in the following, may reflect some lateral stress instabilities. Some of the abnormal patterns, however, may be artifacts due to error in defining the down-dip direction. Under the northern Tonga arc (T1, T2 and T3), for example, Figs 1(b) and 2(b) show that the P-axes of many deepest events trend differently from that of the shallow events. We hence exclude slice T2 from the abnormal list because, under the stereo view of Fig. 2(b), the majority of deep events there have a consistent down-dip compression direction differing from the azimuth of the slice. If the P-axes consistently follow the subduction flow, or in down-dip direction, our use of a constant azimuth in each slice will be faulted in such places of severe azimuthal variation. Hence, these slices are less-weighted in drawing our conclusions on the down-dip stress. Nevertheless, the azimuth of P-axes in most slices, as shown in Fig. 1, generally follow that of the slice.

Figure 6 provides map views of our observations on down-dip stress regimes in slabs in the NW Pacific and Tonga–Kermadec regions. These show the interpreted NDSZ between deeper compression and shallower tension regimes. Down-dip tensional or ambiguous (small κ value) mechanisms take about one third of the data in each of the two regions (Fig. 2). Once again, the general pattern of down-dip compression overlain by down-dip tension or mixed stress is generally confirmed in these two regions (e.g., Fig. 5). This pattern is particularly consistent in the NW Pacific region and under the Kermadec arc. Under the Tonga arc a considerable number of tensional or ambiguous earthquakes appear to occur within the deepest clusters of compressional events.

The most striking feature shown in Fig. 6 is the deep occurrence of tensional or ambiguous earthquakes underneath several major junctions of arcs (e.g., N9, N12 and T6). The P-axes of most of these tensional or ambiguous events are perpendicular to the slab surface, while the corresponding T-axes vary but are consistent within each area (Fig. 2). Some of these events are deeper than 350 km, contrasting with compressional events as shallow as 150 km under adjacent slices. These abnormal stress patterns clearly define distortions or cuts on the NDSZ, suggesting an important influence from lateral stress within the slab, or between slabs, at these localities. The most obvious cuts are underneath the junctions between Hokkaido and Honshu (N9) and between the Japan and Izu–Bonin arcs (N12); both locations are underlain by deep seismicity gaps. The cut between the Tonga and Kermadec arcs (N5 and N6) is mixed with many down-dip compressional earthquakes; however, it corresponds to the regional seismicity gap at intermediate depths as well as the location at which the Louisville Ridge joins the Tonga–Kermadec trench from the southeast (Fig. 6).

Away from regions underneath junctions of arcs, the location of NDSZ [hatched zones shown in Fig. 7(b)] under the Kuril, Japan, Izu–Bonin, Tonga and Kermadec arcs is generally shallower than 200–250 km. In the Mariana arc (N17 to N20) the zone is between 100 and 400 km depth. The zone is quite smooth beneath the central parts of arcs, although it fluctuates in some areas, such as that in N6 of Fig. 6(a) and in T2 of Fig. 6(b). In their 1969 paper Isacks & Molnar already proposed very shallow NDSZ depth under the Tonga, Northern Honshu and Izu–Bonin trenches, based on less than one tenth of the amount of focal mechanism data utilized in the current study. For these regions, the previous view of a 300 km depth transition zone from tension to compression down-dip stress regimes may be a stacked result of solutions under central parts of arcs

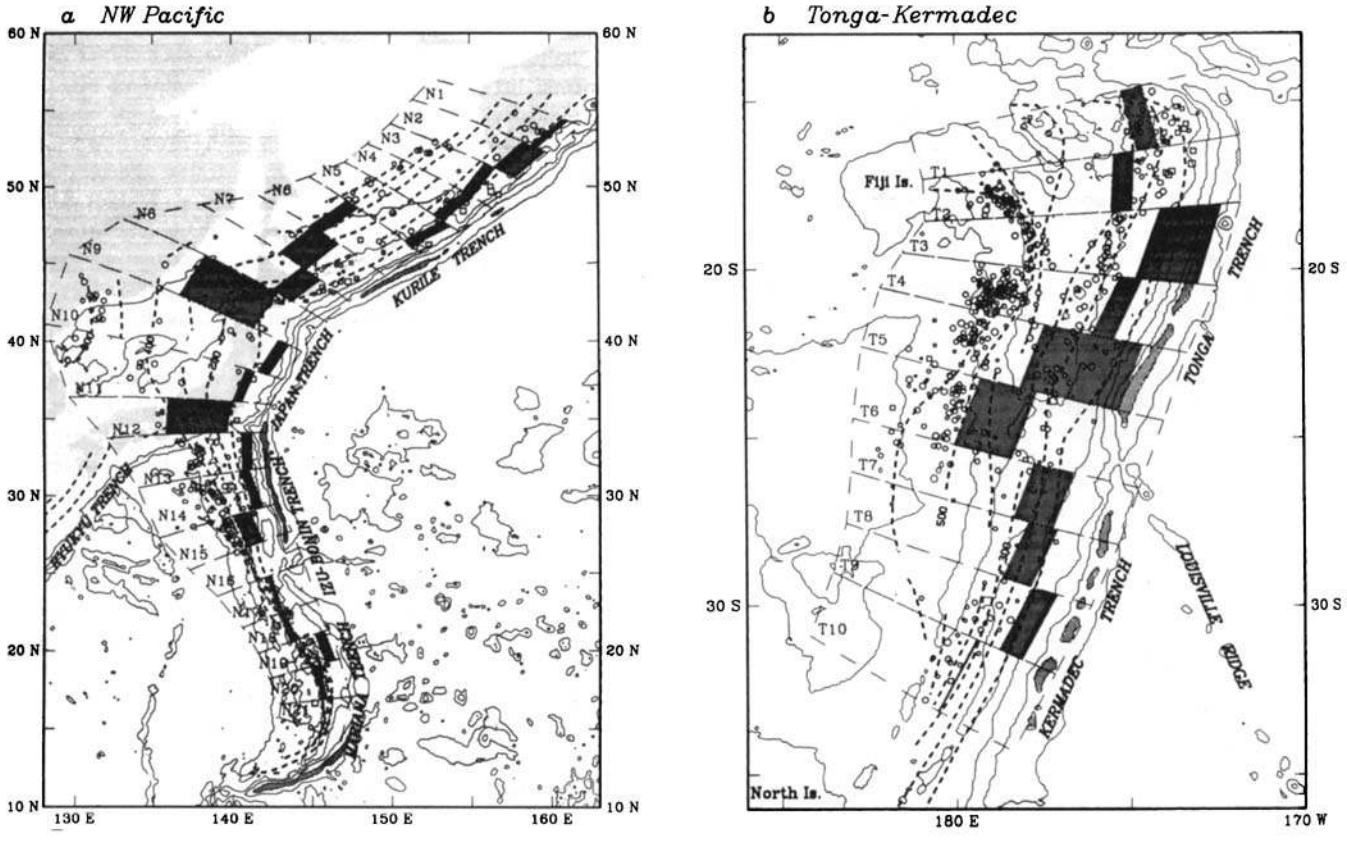

Figure 6. Map views of interpreted NDSZs. (a) NW Pacific; (b) Tonga–Kermadec. Hatched boxes denote the interpreted NDSZs. Circles and squares denote earthquakes of positive κ and negative κ values, respectively, and the size is proportional to the magnitude of κ. See Fig. 1 for other conventions.

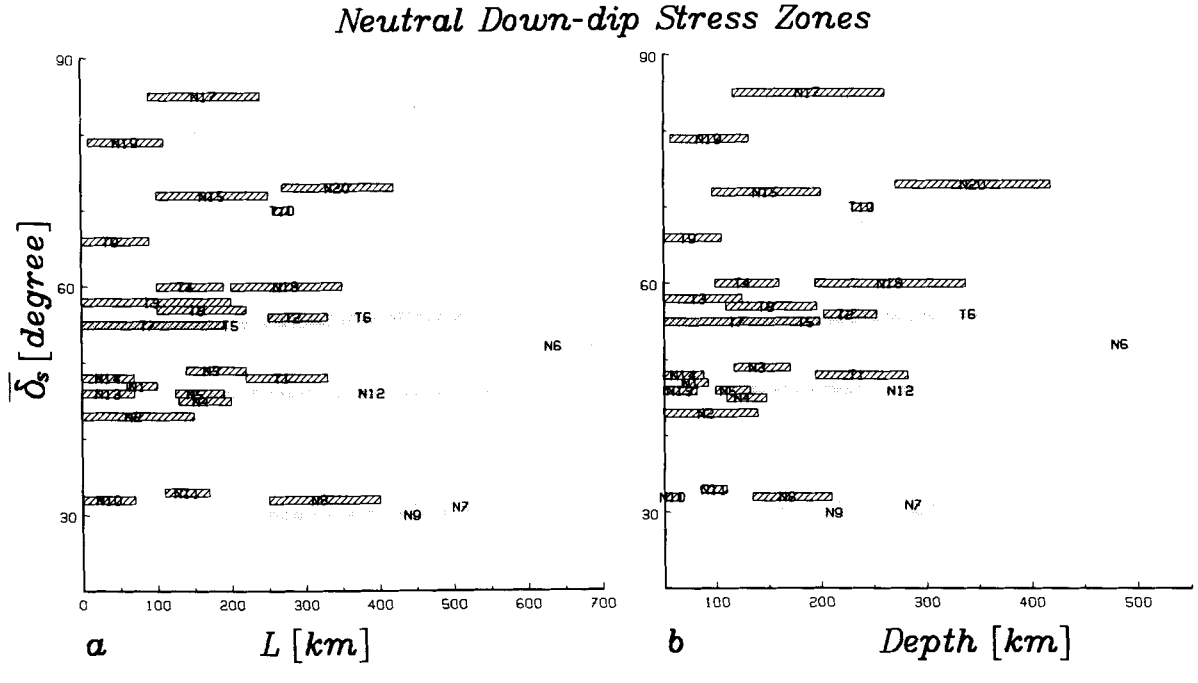

Figure 7. Subducted length L (a), and depth (b), of the NDSZs, respectively, in relation with the average slab plunge $\overline{\delta_s}$. Hatched zones are for slices in the central parts of slabs, grey zones are for several slices near the edge or junction of arcs with abnormal stress patterns. Notice that the 'normal' (hatched) NDSZ is generally deeper with a steeper dip of slab, while the L of NDSZ seems not to depend on the slab.

with generally shallow NDSZ and under junctions of arcs with deep NDSZ.

In the central parts of arcs, at least in these two regions, the depth of the NDSZ appears to correlate with dip (Fig. 7) and, perhaps, also with the topology of the slab. The deepest NDSZ is in the Mariana slab (N20), which dips nearly vertically, while the shallowest NDSZ, probably less than 100 km, is in the shallowly dipping Honshu slab, and in the Izu–Bonin slab (N13–N15) which is flattened to subhorizontal near the base of the upper mantle. The Tonga, Kermadec, and Kuril slabs have intermediate characteristics. The flattening of the Izu–Bonin slab, indicated by fast velocity anomalies, seismicity, and deep *P*-axes (Fig. 3d), occurs around 500 km depth, which is shallower than the deep flattenings of deep *P*-axes beneath the Tonga arc (Fig. 3f).

The slab dip versus *L* plot of the NDSZs in Fig. 7(b), however, shows no evidence of the dependency of the *L* value on the slab dip for slices in the central parts of the arcs. In other words, the NDSZ probably starts at places of more or less the same subducted length along the slab. The variation in slab dip apparently causes its correlation with the depth of NDSZ.

Stress axes and seismic morphology of slabs

The seismic morphology of slabs is mainly inferred from velocity structures. The consistent alignment of *P*-axes with the slab-like fast velocities below several hundred kilometres, however, has the potential to better our understanding about the slab morphology.

'Fingering' of the fast slab-like anomaly, i.e., segmentation of a fast slab into fingers going to different directions near the base of the upper mantle, has been observed in some places by Zhou & Clayton (1987) and Kamiya *et al.* (1988). Although in some cases fingering as well as contortion of the fast slabs can be identified or postulated as artifacts due to things such as along-path smearing, the fingering phenomena appears to be consistent with resolution and error analyses at certain places (Zhou 1988). Many of the deep finger anomalies now have support from orientation of earthquake stress axes. For instance, both fast slab-associated anomalies and deep *P*-axes shown in cross-sections N14 and N15 (Fig. 3d) have a tendency of flattening around 500 km depth, in contrast to the downward-going fast slab anomaly in next cross-section to the south, N16. Another example is shown in cross-sections N4 to N6 beneath the Kuril arc (Fig. 3a); while the fast slab anomaly in N5 illustrates a flattening tendency between 500 to 700 km, the anomaly in the neighbouring cross-sections N4 and N6 appears to be bent downward.

If we assume that the deep *P*-axes consistently follow the subduction flow, they may inform us of the *in situ* down-dip direction and provide an extra guide for interpreting deep slab from tomographic velocity structures in places where the flow direction is not normal to the strike of the arc. Examples of deep *P*-axes which are consistent with themselves but which differ from the normal of the slab strike are seen under the southern Kuril arc. Most deep and intermediate depth earthquakes there seem to have their *P*-axes shifted slightly but systematically to the west (Fig. 1a) from the surface plate motion direction which is approximately perpendicular to the arc.

For some of the deepest earthquakes (e.g., in N14, N17, T7 and T8), however, the fast velocity trend is parallel to one of the nodal planes, which, by definition, bisect the *P*- and *T*-directions. Hence, a possibility arises that earthquakes at the tip of the Wadati–Benioff zone may not necessarily be in down-dip compression, as is also evident from a rather complex situation in the deepest stress axes under the Tonga arc (T2–T6).

DISCUSSION

The NW Pacific and Tonga–Kermadec regions include most of the subducting slabs in the world where earthquakes occur nearly continuously throughout the entire depth range of the upper mantle. Consistent alignment between high-velocity slab anomalies and deep *P*-axes of earthquakes supports the theory that deep compression stress is generally follow the subduction flow. This comparison helps the interpretation of subducting slabs from seismic tomographic structures.

A major result of this research is the pattern found for the NDSZ based on reliable focal mechanism data in the two regions. It is understood that the zone is a loosely defined one, i.e., the down-dip tensional and compressional mechanisms above and below the zone, respectively, could be mixed with a certain amount of different mechanisms. New mechanism data will certainly improve the detailed location of the zone, but the pattern of the zone seems unlikely to be altered much by source relocation.

At depths greater than about 200 km, different types of mechanism solutions in the two regions are spatially separated well (Fig. 6), especially in the NW Pacific, during the time span of the data for more than 28 years. At shallower depths, however, the mixed stress patterns seen in this paper might be attributed to temporal variation in focal mechanisms in response to earthquake cycles of large interplate subduction events (Astiz & Kanamori 1986; Dmowska *et al.* 1988; Astiz *et al.* 1988; Lay *et al.* 1989) and/or existence of double seismic zones in certain places (e.g., Stauder & Maulchin 1976; Hasegawa & Umino 1978). In fact, the presence of heavy mixtures of down-dip compressional and tensional events above the NDSZ beneath the Kuril and Tonga arcs (Fig. 7) is consistent with the presence of temporal variations in mechanisms in these most strongly coupled subduction zones in the two regions (see, e.g., Christensen & Ruff 1988).

The cuts on the NDSZs in the two regions generally agree with segment boundaries previously proposed by Burbach & Frohlich (1986) in their extensive review of lateral changes in Wadati–Benioff zone structure. The anomalous focal mechanisms, i.e., *P*-axes normal to the slab surface, under the two arc junctions in the NW Pacific were observed by these authors with the CMT data available then; they also pointed out the lack of deep seismicity below these places. The state of stress in the slab at these corner locations is apparently highly controlled by lateral geometry of the slab. Hence, a (down-dip) 2-D representation of the stress regime

in slabs should exclude these places as well as the edge of an arc such as the northern end of the Tonga trench.

Christensen & Lay (1988) proposed that the Louisville Ridge as a possibly buoyant feature perturbs the regional stress regime at both intermediate and shallow depths in the slab. Viewed on stress pattern around the cut of the NDSZ at the location (Fig. 6b) and the possibility of southward horizontal shear of deep material, it seems that the perturbation from the subducted Louisville Ridge also contributes to the deep stress anomaly. As mentioned at the end of the previous section, some mixtures of tensional events with compressional events near the bottom of the Tonga seismic zone are probably due to complexity in slab morphology and plate motions. The complexity may be associated with the fact that the Tonga seismic zone possesses the highest level of seismic activity in the world.

Beneath the central parts of arcs in the NW Pacific and Tonga–Kermadec regions the stress patterns in slabs (Fig. 7), except for the Mariana arc, are consistent with the model *c* of Isacks & Molnar (1969), i.e., nearly the entire gravitational load of the slab is supported from below and, perhaps, from the edges; the slab goes into compression at a shallow depth. The depth of NDSZ apparently depends on slab dip and topology, but such a dependency seems to disappear when using *L*, the subducted length along the slab, instead of the depth. Further analysis on this interesting possibility is certainly needed.

The stress patterns in these regions with continuous seismicity over 600 km depth differ considerably from other regions which either lack deep seismicity and show dominant tension (Aleutians and Ryukyus), or have a seismicity truncation at intermediate depth between tensional shallow events and compressional deep events (Peru and Chile). The dominance of tensional events under the central parts of most arcs considered here terminates around 150 km depth; it implies an increase in the stress guide effect (Isacks *et al.* 1968) of slabs in response to encountering resistance at depth. The slab pull force for these oldest slabs is proposed to be large (Spence 1987), making the shallow NDSZ even more interesting.

The earthquake stress information combined with seismic velocity images may help our search for the fate of the deep slabs. Penetrating or trapping of the slab with respect to the upper mantle and lower mantle boundary is sensitive to the density differences between slab and ambient mantle, slab and lower mantle, and dip (Kincaid & Olson 1987). Morphology of the slab and the boundary between the upper and lower mantle depend on the viscosity contrast at the boundary (Gurnis & Hager 1988). There may also be a chemical contrast at the boundary (Anderson 1989). Down-dip compression is usually interpreted as resistance to subduction due to resisting forces on the edges and/or at the tip of the slab. Flattening in seismicity, *P*-axes and the fast velocity slab anomalies near the bottom of the upper mantle beneath the Izu–Bonin and Tonga arcs indicate the flattening behaviour of the deep subducted slab at certain locations. From the current results, the slab seems to flatten to subhorizontal, or at least contorted, at the base of the upper mantle under the Japan, Izu–Bonin, Kermadec arcs and parts of the Tonga arc. High velocities extend to several hundred kilometres below the deepest earthquakes under the Kuril Trench and parts of the Mariana and Tonga arcs.

ACKNOWLEDGMENTS

Thanks are due to Dr Don L. Anderson and Dr R. Dmowska for a critical reading of the manuscript. This research was supported by NSF Grants No. EAR 83-17623 and DOE contract No. DE-F-G03-85ER25009. Contribution No. 4752, Division of Geological and Planetary Sciences, California Institute of Technology.

REFERENCES

Anderson, D. L., 1979. The deep structure of continents, *J. geophys. Res.*, **84,** 7555–7560.

Anderson, D. L., 1987. Thermally induced phase changes, lateral heterogeneity of the mantle, continental roots and deep slab anomalies, *J. geophys. Res.*, **92,** 13 968–13 980.

Anderson, D. L., 1989. Composition of the Earth, *Science*, **243,** 367–370.

Apperson, K. D. & Frohlich, C., 1987. The relationship between Wadati–Benioff zone geometry and P, T and B axes of intermediate and deep focus earthquakes, *J. geophys. Res.*, **92,** 13 821–13 831.

Astiz, L. & Kanamori, H., 1986. Interplate coupling and temporal variation of mechanisms of intermediate-depth earthquakes in Chile, *Bull. seism. Soc. Am.*, **76,** 1614–1622.

Astiz, L., Lay, T. and Kanamori, H., 1988. Large intermediate-depth earthquakes and the subduction process, *Phys. Earth planet. Inter.*, **53,** 80–166.

Billington, S., 1978. The morphology and tectonics of subducted lithosphere in the Tonga–Fiji–Kermadec region from seismicity and focal mechanism solutions, *PhD thesis*, Cornell University, Ithaca, NY.

Burbach, G. V. & Frohlich, C., 1986. Intermediate and deep seismicity and lateral structure of subducted lithosphere in the Circum-Pacific region, *Rev. Geophys.*, **24,** 833–874.

Chandra, U., 1971. Combination of P and S data for determination of earthquake focal mechanism, *Bull. seism. Soc. Am.*, **61,** 1655–1673.

Christensen, D. H. & Ruff, L. J., 1983. Outer-rise earthquakes and seismic coupling, *Geophys. Res. Lett.*, **10,** 697–700.

Christensen, D. H. & Ruff, L. J., 1988. Seismic coupling and outer rise earthquakes, *J. geophys. Res.*, **93,** 13 421–13 444.

Christensen, D. H. & Lay, T., 1988. Large earthquakes in the Tonga region associated with subduction of the Louisville Ridge, *J. geophys. Res.*, **93,** 13 367–13 389.

Dmowska, R., Rice, J. R., Lovison, L. C. & Josell, D., 1988. Stress transfer and seismic phenomena in coupled subduction zones during the earthquake cycle, *J. geophys. Res.*, **93,** 7869–7884.

Dziewonski, A. M. & Woodhouse, J. H., 1983. An experiment in the systematic study of global seismicity: centroid-moment tensor solutions for 201 moderate and large earthquakes of 1981, *J. geophys. Res.*, **88,** 3247–3271.

Dziewonski, A. M., Chou, T. A. & Woodhouse, J. H., 1981. Determination of earthquake source parameters from waveform data for studies of global and regional seismicity, *J. geophys. Res.*, **86,** 2825–2852.

Fujita, K. & Kanamori, H., 1981. Double seismic zone and stresses of intermediate depth earthquakes, *Geophys. J. R. astr. Soc.*, **66,** 131–156.

Giardini, D., 1984. Systematic analysis of deep seismicity: 200 centroid-moment tensor solutions for earthquakes between 1977 and 1980, *Geophys. J. R. astr. Soc.*, **77,** 883–914.

Giardini, D. & Woodhouse, J. H., 1984. Deep seismicity and modes of deformation in Tonga subduction zone, *Nature*, **307,** 505–509.

Giardini, D. & Woodhouse, J. H., 1986. Horizontal shear flow in the mantle beneath the Tonga arc, *Nature*, **319**, 551–555.

Gurnis, M. & Hager, B. H., 1988. Controls on the structure of subducted slabs and the viscosity of the lower mantle, *Nature*, **335**, 317–321.

Hager, B. H., O'Connell, R. J. & Raefsky, A., 1983. Subduction, back-arc spreading and global mantle flow, *Tectonophysics*, **99**, 165–189.

Hasegawa, A. & Umino, N., 1978. Focal mechanisms and the distribution of seismicity in northeastern Japan, *Prog. Abstr. seism. Soc. Japan*, **1**, 34 (in Japanese).

Hirahara, K., 1981. Three-dimensional seismic structure beneath southwest Japan: The subducting Philippine Sea plate, *Tectonophysics*, **79**, 1–41.

Isacks, B. & Molnar, P., 1969. Mantle earthquake mechanisms and sinking of the lithosphere, *Nature*, **223**, 1121–1124.

Isacks, B. & Molnar, P., 1971. Distribution of stresses in the descending lithosphere from a global survey of focal mechanism solution of mantle earthquakes, *Rev. Geophys. Space Phys.*, **9**, 103–174.

Isacks, B., Oliver, J. & Sykes, L. R., 1968. Seismology and the new global tectonics, *J. geophys. Res.*, **73**, 5855–5899.

Isacks, B., Sykes, L. R. & Oliver, J., 1969. Focal mechanisms of deep and shallow earthquakes in the Tonga–Kermadec region and the tectonics of island arcs, *Bull. geol. Soc. Amer.*, **80**, 1443–1470.

Kamiya, S., Miyatake, T. & Hirahara, K., 1988. How deep can we see the high velocity anomalies beneath the Japan Island?, *Geophys. Res. Lett.*, **15**, 828–831.

Kanamori, H. & Given, J. W., 1981. Use of long period surface waves for rapid determination of earthquake source parameters, *Phys. Earth planet. Inter.*, **27**, 8–31.

Kincaid, C. & Olson, P., 1987. An experimental study of subduction and slab migration, *J. geophys. Res.*, **92**, 13 832–13 840.

Lay, T., Astiz, L., Kanamori, H. & Christensen, D. H., 1989. Temporal variation of large intraplate earthquakes in coupled subduction zones, *Phys. Earth planet. Inter.*, 258–312.

Oike, K., 1971. On the nature of the occurrence of intermediate and deep earthquakes. 1. The world wide distribution of the earthquake generating stress, *Bull. Disas. Prev. Res. Inst. Kyoto Univ.*, **20**, 145–182.

Richter, F. M., 1979. Focal mechanisms and seismic energy release of deep and intermediate earthquakes in the Tonga–Kermadec region and their bearing on the depth extent of mantle flow, *J. geophys. Res.*, **84**, 6783–6795.

Sengupta, M. K. & Toksöz, M. N., 1977. The amplitudes of P waves and magnitude corrections for deep focus earthquakes, *J. geophys. Res.*, **82**, 2971–2980.

Spence, W., 1987. Slab pull and the seismotectonics of subducting lithosphere, *Rev. Geophys.*, **25**, 55–69.

Stauder, W. & Maulchin, L., 1976. Fault motion in the larger earthquakes of the Kurile–Kamchatka arc and the Kurile–Hokkaido corner, *J. geophys. Res.*, **81**, 2297–2308.

Toksöz, M. N., Minear, J. W. & Julian, B. R., 1971. Temperature field and geophysical effects of a down-going slab, *J. geophys. Res.*, **76**, 1113–1138.

Toksöz, M. N., Sleep, N. H. & Smith, A. T., 1973. Evolution of the downgoing lithosphere and the mechanisms of deep focus earthquakes, *Geophys. J. R. astr. Soc.*, **35**, 285–310.

Utsu, T., 1971. Seismological evidence for anomalous structure of island arcs with special reference to the Japanese region, *Rev. Geophys. Space Phys.*, **9**, 839–890.

Vassiliou, M. S., 1984. The state of stress in subducting slabs as revealed by earthquakes analyzed by moment tensor inversion, *Earth planet. Sci. Lett.*, **69**, 195–202.

Vassiliou, M. S. & Hager, B. H., 1988. Subduction zone earthquakes and stress in slabs, *Pageoph*, **128**, 547–624.

Zhou, H., 1988. How well can we resolve the deep seismic slab with seismic tomography?, *Geophys. Res. Lett.*, **15**, 1425–1428.

Zhou, H., 1990. Mapping of P-wave slab anomalies beneath the Tonga, Kermadec and New Hebrides arcs, *Phys. Earth planet. Inter.*, **61**, 199–229.

Zhou, H. & Clayton, R. W., 1987. Travel-time inversions for P and S velocities beneath the northwest edge of the Pacific: slab fingering?, *Abstract, EOS, Trans. Am. geophys. Un.*, **68**, 1379.

Zhou, H. & Clayton, R. W., 1988. P wave velocities around subduction zones in the southwest Pacific, *Abstract, EOS, Trans. Am. geophys. Un.*, **69**, 398.

Zhou, H. & Clayton, R. W., 1990. P and S wave travel-time inversions for subducting slab under the island arc of the Northwest Pacific, *J. geophys. Res.*, **95**, 6829–6852.

APPENDIX

Table 1. Compilation of deep and intermediate-depth focal mechanisms.

	Event Information					Slab			Angle from down-dip			T Axis		P Axis		
	Date	Lat. (°)	Lon. (°)	Depth (km)	m_b	δ_s (°)	L (km)	κ	η_T (°)	η_B (°)	η_P (°)	δ (°)	θ (°)	δ (°)	θ (°)	Ref
N1	θ_s=306.1	$\bar{\delta}_s$=47														
1	11/ 6/77	53.55N	159.81E	94.0	5.2	37	83	0.75	78	80	15	62	98	27	292	CMT
2	7/25/60	54.00N	159.00E	100.0	6.9	45	154	0.89	87	68	3	26	182	46	301	FK
3	11/24/71	52.90N	159.19E	106.0	7.3	40	99	-0.83	9	85	81	49	300	41	120	ALK
4	11/14/82	52.98N	158.70E	110.0	5.9	42	111	0.81	81	81	12	37	142	53	318	CMT
5	6/ 1/84	53.67N	159.32E	114.8	5.3	45	130	0.86	86	73	17	40	111	43	330	CMT
6	8/25/85	53.71N	158.96E	134.7	5.3	45	153	0.87	82	88	7	49	102	39	302	CMT
7	7/ 6/87	53.09N	158.45E	157.5	—	47	173	0.81	81	81	12	33	138	57	320	CMT
8	7/24/83	53.85N	158.39E	177.4	6.1	50	223	0.87	83	82	9	45	139	43	298	CMT
9	4/16/87	55.01N	158.00E	333.1	5.0	61	405	0.61	70	85	19	21	34	51	277	CMT
N2	θ_s=309.1	$\bar{\delta}_s$=43														
1	4/25/83	51.33N	156.93E	100.6	5.2	35	83	0.61	83	57	32	58	98	32	270	CMT
2	10/13/81	51.48N	157.44E	112.2	5.3	42	113	-0.15	55	42	69	20	248	66	102	CMT
3	1/ 7/80	51.32N	156.67E	121.5	5.6	31	49	0.67	73	89	16	21	182	40	292	CMT
4	8/22/79	52.27N	157.33E	126.7	5.6	42	110	0.75	77	86	13	44	67	30	303	CMT
5	3/ 2/86	51.67N	156.91E	126.3	5.6	42	120	0.57	69	83	21	23	105	64	314	CMT
6	12/26/64	51.90N	156.70E	145.0	—	46	172	0.96	88	83	6	45	120	45	300	IM
7	3/31/87	53.09N	156.34E	191.2	5.2	47	260	0.61	83	57	33	28	195	17	294	CMT
8	3/18/64	52.60N	153.70E	424.0	—	52	505	0.84	82	83	10	45	140	45	320	BJ
9	8/ 1/65	52.73N	153.48E	446.0	—	48	534	0.58	74	65	26	24	215	23	316	OI

Table 1. (*continued*)

	Event Information					Slab			Angle from down-dip			T Axis		P Axis		
	Date	Lat. (°)	Lon. (°)	Depth (km)	m_b	δ_s (°)	L (km)	κ	η_T (°)	η_B (°)	η_P (°)	δ (°)	θ (°)	δ (°)	θ (°)	Ref.
N3	θ_s=311.7	$\bar{\delta}_s$=49														
1	9/19/87	50.37N	155.79E	72.4	—	37	124	-0.85	11	81	82	32	300	58	114	CMT
2	8/14/78	49.87N	156.28E	77.8	5.8	32	63	-0.83	24	65	89	30	340	58	137	CMT
3	9/ 8/87	49.46N	156.79E	105.1	—	21	34	-0.59	26	67	75	28	283	52	150	CMT
4	2/ 5/66	50.00N	155.40E	121.0	—	38	149	-0.49	26	75	67	54	280	28	141	IM
5	5/12/77	50.16N	154.99E	128.3	5.3	38	143	0.62	71	86	18	31	148	55	298	CMT
6	8/ 8/82	50.91N	156.07E	136.9	—	42	180	-0.74	22	69	82	47	281	40	127	CMT
7	10/28/78	50.25N	155.69E	139.5	5.5	37	123	-0.62	18	88	71	56	317	33	129	CMT
8	1/29/63	49.70N	155.00E	143.0	—	38	159	-0.76	15	80	79	48	328	40	122	IM
9	9/21/77	51.75N	155.21E	212.7	5.6	53	254	0.89	86	77	13	33	129	54	334	CMT
10	5/15/84	50.99N	153.78E	308.5	5.0	55	380	0.27	56	81	34	1	121	72	28	CMT
11	10/12/67	52.20N	152.50E	476.0	—	59	615	0.82	85	69	17	20	93	46	331	IM
12	8/ 5/86	53.02N	153.32E	511.5	4.7	57	653	0.81	85	70	20	30	90	60	271	CMT
13	8/15/87	52.19N	152.35E	518.8	—	57	655	0.79	81	76	16	25	196	41	310	CMT
14	12/30/79	52.53N	152.26E	548.7	5.4	66	704	0.69	79	69	23	33	115	54	270	CMT
15	8/30/70	52.36N	151.73E	625.0	—	72	777	0.76	77	89	12	5	130	85	310	ST
N4	θ_s=315.4	$\bar{\delta}_s$=45														
1	3/28/86	48.81N	154.77E	74.7	5.2	30	90	-0.81	16	73	83	14	312	31	214	CMT
2	9/ 3/78	49.45N	154.36E	117.6	5.5	33	138	0.85	81	88	8	47	150	41	311	CMT
3	2/19/86	48.58N	153.40E	119.2	5.3	33	174	0.69	74	83	16	38	114	45	331	CMT
4	3/22/72	49.06N	153.57E	134.0	6.8	40	204	0.66	73	82	17	30	114	58	311	SM
5	12/ 1/67	49.50N	154.40E	136.0	—	37	194	-0.71	15	87	75	51	325	36	117	IM
6	5/30/85	49.14N	154.10E	150.7	5.5	34	181	-0.93	3	89	85	31	316	57	159	CMT
7	8/22/84	48.99N	153.52E	153.8	5.2	44	244	0.59	69	85	20	21	108	63	327	CMT
8	9/ 1/65	51.29N	150.70E	501.0	—	56	675	0.47	69	66	30	7	252	35	347	OI
9	6/ 4/84	51.23N	150.75E	505.6	5.2	57	683	0.60	79	62	29	30	76	29	327	CMT
10	6/10/80	51.55N	150.64E	569.1	5.2	69	755	0.45	67	70	30	30	61	60	242	CMT
N5	θ_s=318.5	$\bar{\delta}_s$=46														
1	4/20/78	46.78N	151.90E	78.7	5.5	30	129	0.93	87	79	10	40	74	35	308	CMT
2	8/ 4/64	46.60N	151.40E	86.0	—	30	160	0.84	81	85	9	51	133	39	313	IM
3	3/ 3/87	46.33N	152.07E	96.8	5.9	26	91	-0.83	21	68	87	25	295	60	151	CMT
4	8/28/83	46.20N	151.54E	97.5	5.5	29	123	0.10	71	35	61	38	112	40	243	CMT
5	10/ 4/78	46.27N	151.72E	98.9	5.7	29	120	-0.70	16	82	75	23	302	1	211	CMT
6	12/10/77	47.59N	152.84E	119.0	5.2	30	150	0.27	89	31	58	15	219	26	121	CMT
7	7/20/79	47.46N	152.31E	132.1	5.2	30	167	-0.02	66	32	69	30	37	37	154	CMT
8	10/30/83	47.57N	153.01E	133.7	—	30	180	-0.62	19	81	71	49	309	41	132	CMT
9	7/19/86	47.22N	151.13E	153.4	5.9	39	231	0.74	76	87	13	34	114	53	322	CMT
10	6/19/77	47.15N	151.09E	157.4	5.6	30	184	0.78	79	81	13	37	94	44	317	CMT
11	12/20/77	48.59N	153.02E	159.1	5.8	31	202	0.58	71	75	23	37	116	53	305	CMT
12	7/10/78	48.79N	150.11E	343.7	5.1	64	486	0.95	89	78	11	25	123	64	291	CMT
13	6/21/78	48.31N	148.61E	402.0	5.9	58	545	0.31	76	44	48	44	121	35	253	CMT
14	1/ 4/87	49.78N	149.28E	505.4	5.1	53	684	0.97	89	82	7	28	96	58	308	CMT
15	5/18/87	49.19N	147.70E	551.7	6.0	53	755	0.97	88	89	1	38	140	52	320	CMT
16	1/29/82	49.15N	147.85E	553.8	5.2	53	752	0.92	86	81	9	21	73	44	321	CMT
17	1/25/79	50.50N	148.90E	587.6	5.4	55	810	0.80	79	85	11	41	106	47	306	CMT
18	7/14/87	49.59N	147.67E	588.6	—	54	805	0.44	74	57	37	51	142	30	279	CMT
19	4/20/84	50.03N	148.76E	592.8	6.0	54	803	0.90	84	86	5	29	154	60	323	CMT
20	11/27/82	50.17N	147.79E	628.0	5.6	57	886	-0.07	48	62	54	68	82	22	261	CMT
N6	θ_s=318.3	$\bar{\delta}_s$=52														
1	9/23/87	45.70N	149.57E	130.9	—	31	144	0.38	61	83	30	3	192	31	283	CMT
2	1/29/78	45.97N	149.15E	159.0	5.5	31	157	-0.27	34	84	56	46	358	14	103	CMT
3	7/ 8/87	46.23N	149.53E	159.4	—	40	201	0.58	73	71	25	30	117	59	290	CMT
4	8/17/61	46.40N	149.30E	160.0	6.7	45	222	0.63	80	62	29	35	130	50	275	FK
5	6/10/79	46.92N	148.16E	271.0	4.9	50	345	-0.60	20	86	70	46	348	21	234	CMT
6	4/23/84	47.46N	146.73E	417.0	6.0	57	563	-0.30	34	77	58	80	52	7	281	CMT
7	2/23/85	47.37N	145.65E	429.3	5.4	58	585	0.49	77	56	37	44	137	36	272	CMT
8	11/22/66	48.00N	146.80E	452.0	—	58	605	-0.09	44	71	51	75	102	15	280	IM
9	12/22/80	48.17N	146.21E	485.1	5.4	66	662	-0.17	41	69	55	69	102	21	269	CMT
10	2/ 6/81	48.30N	146.35E	517.1	5.3	67	675	-0.03	57	48	59	55	134	21	258	CMT
11	2/ 1/84	49.03N	146.61E	581.3	6.0	72	766	0.29	57	82	33	50	133	39	328	CMT
N7	θ_s=317.1	$\bar{\delta}_s$=31														
1	3/14/86	43.94N	147.65E	78.3	5.8	26	151	-0.80	16	74	82	28	336	54	115	CMT
2	7/ 4/79	43.95N	146.70E	80.5	6.0	26	178	0.91	89	72	16	59	170	21	300	CMT
3	4/ 5/86	44.47N	147.86E	83.0	5.3	25	142	-0.48	28	72	67	0	150	27	240	CMT
4	6/20/83	45.00N	147.54E	93.1	—	26	232	-0.26	42	59	64	8	357	18	90	CMT
5	4/11/83	44.30N	147.78E	101.5	5.7	26	153	-0.25	45	53	66	38	10	40	140	CMT

Table 1. (*continued*)

	Event Information					Slab			Angle from down-dip			T Axis		P Axis		
	Date	Lat. (°)	Lon. (°)	Depth (km)	m_b	δ_s (°)	L (km)	κ	η_T (°)	η_B (°)	η_P (°)	δ (°)	θ (°)	δ (°)	θ (°)	Ref
6	5/14/79	44.76N	147.59E	108.5	5.6	26	224	-0.04	52	55	56	58	19	19	256	CMT
7	12/10/85	44.21N	146.90E	120.0	5.3	26	188	-0.33	44	50	73	26	7	46	127	CMT
8	3/27/85	44.39N	146.70E	142.3	6.0	27	241	0.06	52	66	47	37	19	18	123	CMT
9	5/18/87	44.45N	147.06E	145.1	5.3	27	276	-0.25	52	39	77	61	19	26	228	CMT
10	1/26/85	44.99N	146.57E	172.7	5.4	27	303	0.21	56	72	39	32	23	7	117	CMT
11	12/ 6/78	44.59N	146.58E	181.0	6.7	27	336	0.35	59	83	31	18	22	28	282	CMT
12	10/25/65	44.20N	145.30E	181.0	—	27	317	-0.39	31	75	63	50	346	36	139	OI
13	10/25/65	44.20N	145.30E	181.0	—	27	317	-0.39	31	75	63	50	346	36	139	IM
14	10/18/85	46.30N	146.29E	277.1	6.0	46	464	-0.64	29	60	82	39	357	49	156	CMT
15	6/30/64	46.60N	144.60E	383.0	—	44	624	-0.43	43	48	81	43	18	36	151	IM
16	8/ 1/65	46.82N	143.84E	384.0	—	43	670	0.67	85	57	27	27	207	17	306	OI
N8	θ_s=313.5	$\overline{\delta_s}$=32														
1	5/31/86	43.33N	145.60E	70.7	5.4	27	177	-0.49	44	45	88	28	4	59	157	CMT
2	12/14/79	42.82N	144.30E	72.6	5.5	27	182	-0.19	54	40	73	25	15	65	202	CMT
3	6/23/64	43.20N	146.20E	76.0	—	20	147	-0.16	43	63	57	48	356	36	142	IM
4	10/28/78	42.68N	144.22E	82.0	5.1	28	237	-0.01	54	54	55	55	22	24	251	CMT
5	9/19/67	43.00N	145.20E	84.0	—	28	191	-0.24	44	56	65	50	6	35	148	IM
6	3/16/84	42.94N	145.52E	84.0	5.6	19	129	0.51	66	87	24	84	269	4	139	CMT
7	5/23/78	42.74N	144.70E	87.8	5.6	28	193	-0.02	59	45	61	36	25	32	142	CMT
8	3/10/85	43.46N	145.99E	101.2	5.3	27	179	-0.43	29	76	64	49	340	37	129	CMT
9	2/18/80	43.66N	145.90E	124.3	5.4	28	208	-0.67	32	58	86	28	350	62	163	CMT
10	1/19/69	45.00N	143.20E	204.0	6.5	34	472	0.20	53	88	36	28	16	22	274	Cn
11	7/14/82	45.62N	142.57E	328.7	—	31	599	0.33	58	89	31	43	28	11	287	CMT
12	1/ 6/85	45.87N	143.36E	332.5	5.3	32	571	0.09	48	86	41	38	14	14	273	CMT
13	5/ 7/87	46.77N	139.21E	442.2	6.1	41	894	0.25	55	84	34	53	38	18	283	CMT
N9	θ_s=307.3	$\overline{\delta_s}$=30														
1	2/24/77	42.39N	142.51E	73.0	5.3	23	201	-0.45	34	61	72	10	137	17	230	CMT
2	3/19/72	40.83N	141.90E	76.0	6.0	20	137	0.86	82	87	7	2	46	24	315	SM
3	12/ 2/81	40.91N	142.55E	83.3	5.8	19	119	-0.11	52	48	62	3	176	27	84	CMT
4	6/ 1/85	41.57N	142.10E	84.6	5.2	21	189	-0.11	40	86	49	59	328	24	108	CMT
5	1/14/87	42.56N	142.88E	89.4	6.5	23	204	-0.58	38	52	87	38	349	52	177	CMT
6	5/29/83	42.72N	143.43E	93.1	5.3	21	187	0.12	74	32	61	45	90	40	237	CMT
7	9/12/81	42.74N	143.22E	105.3	4.9	20	170	-0.00	50	62	51	12	167	3	258	CMT
8	6/21/84	42.64N	142.53E	106.5	5.5	26	213	0.22	75	40	53	37	38	24	148	CMT
9	3/ 6/84	42.64N	142.88E	106.2	5.5	21	193	-0.23	51	43	73	37	5	48	153	CMT
10	5/29/82	42.72N	143.18E	118.1	5.7	20	169	-0.34	41	54	70	49	345	41	164	CMT
11	1/23/81	42.52N	142.12E	120.9	6.3	28	231	-0.76	24	66	85	35	335	55	146	CMT
12	3/17/83	41.80N	140.76E	124.6	5.3	33	328	0.76	77	88	12	63	85	22	301	CMT
13	5/21/64	42.90N	141.90E	129.0	—	28	282	0.73	87	57	24	64	120	22	333	OI
14	12/ 6/85	43.14N	141.06E	152.1	5.1	34	364	0.59	87	52	38	50	170	40	355	CMT
15	7/ 4/67	43.20N	142.50E	160.0	—	28	272	-0.52	41	49	86	45	356	43	193	IM
16	8/20/66	43.10N	140.60E	163.0	—	34	384	0.87	87	72	17	53	120	33	328	IM
17	7/28/81	41.68N	139.97E	177.8	5.4	34	348	-0.36	38	61	67	10	340	78	133	CMT
18	6/21/79	43.89N	139.70E	241.5	5.4	35	507	0.52	79	56	35	65	125	20	344	CMT
19	5/ 8/81	42.66N	139.13E	248.0	6.0	35	538	-0.05	71	21	79	16	26	44	132	CMT
20	5/31/81	44.56N	137.27E	280.8	5.4	35	682	-0.07	53	52	59	22	7	19	104	CMT
21	2/20/31	44.90N	135.80E	350.0	—	32	841	0.88	83	87	6	27	207	27	311	HIM
N10	θ_s=298.3	$\overline{\delta_s}$=32														
1	6/ 8/77	38.54N	141.49E	81.6	5.5	18	80	0.70	74	88	15	32	21	11	284	CMT
2	11/26/80	40.39N	141.31E	91.9	5.8	29	217	0.74	76	86	13	37	78	43	303	CMT
3	11/27/80	40.37N	141.28E	108.7	5.4	29	207	0.54	73	67	29	45	34	33	264	CMT
4	3/28/85	40.30N	140.35E	168.8	6.1	32	320	-0.05	68	26	75	24	219	63	65	CMT
5	6/ 9/80	40.80N	139.86E	172.1	5.6	32	348	0.76	87	63	26	55	83	19	324	CMT
6	7/27/65	40.21N	139.36E	195.0	—	32	378	0.86	86	66	7	60	125	30	306	OI
7	10/21/78	41.23N	135.47E	380.9	5.1	39	763	0.61	70	88	19	69	96	20	297	CMT
8	6/15/78	43.35N	135.37E	381.6	5.2	37	804	0.91	86	82	9	37	57	29	301	CMT
9	2/11/87	43.15N	132.14E	504.2	5.4	32	1083	0.48	67	73	28	6	177	21	269	CMT
10	2/ 3/77	42.97N	130.93E	504.7	5.0	31	1180	0.49	65	89	24	30	16	21	274	CMT
11	9/28/83	41.21N	132.44E	519.9	5.1	32	1044	0.69	74	86	15	18	21	24	283	CMT
12	12/25/79	43.23N	131.19E	543.0	5.0	31	1151	0.93	85	89	4	52	97	36	299	CMT
13	11/27/81	42.88N	131.11E	546.2	5.7	31	1164	0.75	81	71	20	42	48	38	274	CMT
14	8/ 6/65	41.39N	131.34E	554.0	—	32	1079	0.66	75	66	14	14	20	26	283	OI
15	4/10/69	42.02N	131.07E	564.0	—	31	1138	0.49	65	83	25	17	10	32	268	ST
16	4/15/84	42.98N	131.03E	566.8	5.0	31	1161	0.75	79	75	17	39	79	32	319	CMT
17	9/ 9/77	42.98N	131.36E	567.7	4.9	32	1117	0.69	75	80	17	7	15	22	282	CMT
18	10/ 8/83	44.22N	130.66E	572.8	5.7	31	1204	0.47	74	59	35	70	80	20	261	CMT
19	1/31/79	42.78N	131.20E	575.2	5.7	31	1189	0.88	84	79	11	38	49	21	301	CMT

Table 1. (*continued*)

	Date	Event Information Lat. (°)	Lon. (°)	Depth (km)	m_b	Slab δ_s (°)	L (km)	κ	Angle from down-dip η_T (°)	η_B (°)	η_P (°)	T Axis δ (°)	θ (°)	P Axis δ (°)	θ (°)	Ref.
20	3/ 9/77	41.61N	130.88E	578.6	5.9	32	1084	0.92	85	88	4	58	86	29	295	CMT
21	1/ 3/57	43.80N	130.60E	593.0	—	31	1217	0.95	88	80	9	55	86	33	287	Hi
22	8/16/79	41.81N	130.79E	604.4	6.1	32	1112	0.86	82	88	7	59	76	26	294	CMT
N11	θ_s=284.7	$\overline{\delta_s}$=33														
1	8/23/82	37.55N	141.35E	89.1	—	25	99	-0.72	29	60	87	38	316	47	169	CMT
2	7/28/85	37.34N	140.41E	109.0	5.3	29	164	0.80	79	87	10	41	145	36	275	CMT
3	10/ 7/85	38.40N	140.29E	114.8	5.1	29	191	0.50	83	50	40	54	101	25	330	CMT
4	3/ 4/59	37.60N	138.70E	219.0	—	34	362	-0.16	44	75	57	7	246	23	350	Ic
5	5/28/79	37.41N	136.77E	279.3	5.1	33	520	0.95	87	84	6	37	48	31	292	CMT
6	2/ 3/82	36.84N	135.56E	341.6	5.4	35	711	0.67	81	64	28	1	184	9	274	CMT
7	3/11/84	38.36N	135.50E	353.8	5.3	35	700	0.86	84	77	13	57	132	33	301	CMT
8	3/ 6/78	38.25N	133.97E	430.1	5.1	35	803	0.71	85	61	28	42	145	22	256	CMT
9	1/18/80	37.72N	133.41E	432.5	5.5	35	833	0.78	87	64	25	52	115	31	255	CMT
10	5/31/35	38.60N	134.20E	450.0	—	35	810	0.89	84	85	7	7	27	41	291	Hi
11	12/11/64	38.90N	130.22E	551.0	—	32	1140	0.26	58	77	37	18	73	34	330	OI
12	1/24/64	38.75N	129.54E	557.0	—	32	1193	0.74	79	77	20	61	149	27	308	OI
13	1/24/64	38.80N	129.50E	557.0	—	32	1198	0.82	81	85	10	56	157	26	294	IM
14	10/ 8/60	40.20N	130.00E	605.0	—	29	1099	0.89	86	78	12	56	118	34	298	Hi
N12	θ_s=273.8	$\overline{\delta_s}$=46														
1	2/27/83	35.87N	139.95E	73.4	5.9	33	114	-0.10	41	86	49	74	286	15	85	CMT
2	3/15/83	34.78N	137.57E	74.0	5.4	—	—	—	—	—	—	8	236	70	124	CMT
3	9/23/80	35.95N	139.63E	75.3	5.4	35	128	0.19	57	66	42	16	66	74	239	CMT
4	3/12/80	34.87N	140.42E	80.5	5.5	31	102	-0.65	26	65	79	47	246	43	63	CMT
5	8/12/82	34.87N	139.48E	113.0	5.3	38	204	0.38	73	53	41	23	50	16	313	CMT
6	10/ 4/85	35.76N	140.00E	113.7	5.8	35	163	0.81	80	89	10	37	57	44	281	CMT
7	5/14/54	36.00N	137.40E	225.0	—	46	384	-0.19	60	29	82	29	198	49	71	RA
8	10/ 8/78	36.02N	137.14E	257.6	5.3	46	412	-0.58	29	64	77	39	234	51	55	CMT
9	11/14/86	35.95N	136.87E	261.7	5.1	47	453	-0.43	44	45	84	37	213	46	70	CMT
10	10/26/52	34.30N	137.50E	290.0	—	46	421	0.82	88	67	22	8	178	24	272	Hi
11	6/ 2/29	34.50N	137.20E	350.0	—	47	483	0.69	74	87	15	58	98	32	278	HIM
12	8/13/67	35.30N	135.30E	357.0	—	49	612	-0.25	47	50	69	28	330	59	124	IM
13	5/ 5/32	34.60N	135.30E	360.0	—	49	612	0.66	80	65	26	45	55	45	235	HIM
14	6/23/65	35.51N	135.56E	363.0	—	49	595	0.21	83	87	70	2	192	60	98	OI
15	3/31/80	35.45N	135.47E	367.1	5.8	49	600	0.06	89	14	75	19	162	48	50	CMT
16	0/ 0/29	35.00N	137.00E	386.0	—	50	525	0.86	82	87	5	15	150	50	265	OI
N13	θ_s=266.3	$\overline{\delta_s}$=46														
1	10/20/80	33.08N	140.38E	81.0	5.6	36	74	0.41	64	74	30	28	79	54	303	CMT
2	11/17/77	33.64N	139.87E	103.6	5.5	39	91	0.37	84	40	49	42	59	14	315	CMT
3	11/29/83	32.59N	139.94E	126.1	5.7	49	164	0.51	80	54	37	31	79	40	318	CMT
4	4/26/87	31.85N	139.53E	147.3	5.2	57	192	0.06	87	16	74	35	80	16	181	CMT
5	5/ 1/65	33.48N	138.97E	230.0	—	59	275	0.89	87	88	21	27	72	52	302	OI
6	6/25/36	32.40N	138.00E	300.0	—	56	394	0.77	80	76	16	43	76	43	282	HIM
7	7/16/87	33.04N	137.97E	301.4	—	56	393	0.41	67	66	33	53	52	25	283	CMT
8	1/ 6/81	32.88N	138.34E	304.5	5.4	56	391	0.71	88	58	31	27	50	34	299	CMT
9	6/11/64	33.10N	137.89E	341.0	—	45	430	0.86	82	87	8	3	10	43	277	OI
10	4/20/42	33.00N	137.80E	350.0	—	44	443	0.96	89	80	9	45	100	45	280	HIM
11	3/ 5/81	32.10N	137.90E	357.4	5.1	44	451	0.69	74	86	16	58	116	30	275	CMT
12	1/ 1/84	33.40N	137.32E	383.6	6.5	37	524	0.82	80	88	9	57	50	28	265	CMT
13	4/22/80	32.11N	137.57E	388.1	5.7	38	503	0.82	80	84	10	38	57	44	278	CMT
14	3/10/66	32.20N	137.70E	390.0	—	42	482	0.85	83	79	12	53	101	33	255	KS
15	10/ 7/86	31.86N	137.65E	395.6	5.0	37	508	0.97	89	81	7	53	86	37	276	CMT
16	3/ 7/78	31.96N	137.61E	434.4	6.9	37	523	0.79	79	83	12	57	46	30	254	CMT
N14	θ_s=257.3	$\overline{\delta_s}$=48														
1	1/15/64	29.20N	141.10E	80.0	—	34	64	-0.06	74	16	86	66	34	12	154	KS
2	12/19/80	30.58N	140.64E	90.3	6.2	34	60	0.71	87	59	30	57	91	31	293	CMT
3	9/ 6/82	29.31N	140.28E	155.6	6.6	62	155	0.42	76	53	40	11	51	39	312	CMT
4	9/14/87	30.36N	139.77E	167.1	—	69	195	0.41	75	53	40	35	90	43	319	CMT
5	1/14/79	29.25N	139.55E	363.9	4.9	66	385	0.69	81	66	24	29	111	59	311	CMT
6	4/24/84	30.79N	138.37E	394.8	6.2	54	445	0.83	83	75	15	24	44	50	282	CMT
7	4/10/85	29.98N	138.79E	398.1	5.8	54	450	0.88	83	85	7	26	52	58	270	CMT
8	1/11/78	29.97N	138.75E	412.2	5.3	53	464	0.73	89	59	30	30	41	58	202	CMT
9	5/19/87	29.85N	139.04E	421.5	5.5	54	444	0.20	55	74	39	68	53	17	271	CMT
10	4/12/65	30.21N	138.68E	425.0	—	51	474	0.87	83	82	7	24	36	46	265	OI
11	4/12/65	30.20N	138.70E	428.0	—	51	475	0.67	74	79	19	51	48	32	263	KS
12	8/19/65	30.29N	138.58E	443.0	—	44	492	0.82	84	80	21	14	10	27	273	OI
13	4/ 4/32	30.60N	139.50E	445.0	—	54	440	0.79	79	82	12	43	53	43	263	HIM

Table 1. (*continued*)

	Event Information					Slab			Angle from down-dip			T Axis		P Axis		
	Date	Lat. (°)	Lon (°)	Depth (km)	m_b	δ_s (°)	L (km)	κ	η_T (°)	η_B (°)	η_P (°)	δ (°)	θ (°)	δ (°)	θ (°)	Ref.
14	3/ 6/84	29.36N	138.87E	446.0	6.3	51	475	0.90	85	84	7	39	44	44	261	CMT
15	6/12/82	30.40N	138.20E	447.5	5.5	43	520	0.88	85	77	13	50	64	39	240	CMT
16	1/16/86	29.80N	138.65E	455.7	5.2	53	465	0.81	87	67	22	32	37	37	280	CMT
17	3/ 5/84	28.72N	139.18E	455.6	5.1	51	473	0.90	87	77	13	35	38	54	236	CMT
18	6/23/82	29.03N	138.59E	466.8	—	43	528	0.48	65	83	25	19	57	60	290	CMT
19	2/18/56	30.20N	138.10E	475.0	—	42	544	0.81	80	82	11	4	338	35	246	RA
20	1/ 1/77	30.66N	137.06E	476.5	5.2	38	609	0.68	77	73	21	29	354	45	230	CMT
21	5/31/81	30.69N	137.60E	482.9	5.1	39	564	0.79	82	74	17	14	349	53	239	CMT
22	5/ 7/64	30.59N	137.84E	485.0	—	41	553	0.65	76	80	27	5	181	65	282	OI
23	4/20/77	30.60N	137.48E	495.4	5.5	38	579	0.13	78	29	62	12	142	70	15	CMT
24	7/18/78	30.40N	137.10E	497.8	4.9	38	601	0.62	72	79	20	14	336	45	231	CMT
25	3/19/87	29.27N	137.87E	524.0	5.3	38	614	0.48	71	64	32	24	342	7	249	CMT
26	12/29/77	28.53N	138.37E	538.4	5.2	38	584	0.64	83	60	31	24	358	58	220	CMT
27	7/ 4/82	27.91N	136.92E	551.8	6.3	36	712	0.06	55	59	49	32	189	50	326	CMT
N15	θ_s=250.6	$\overline{\delta_s}$=72														
1	6/ 5/85	28.56N	141.03E	79.7	5.1	33	71	-0.40	44	47	79	66	199	24	13	CMT
2	12/11/79	28.88N	140.70E	124.7	6.1	41	134	0.26	85	34	56	44	74	25	317	CMT
3	4/16/80	27.99N	140.14E	231.8	5.4	76	296	-0.05	48	63	52	30	221	38	338	CMT
4	5/21/77	27.58N	140.00E	345.2	5.1	86	416	0.65	78	67	25	15	64	62	302	CMT
5	12/16/80	28.49N	139.66E	384.2	5.3	86	448	0.59	82	57	33	11	77	56	331	CMT
6	9/ 7/79	28.31N	139.58E	422.9	4.9	86	486	0.92	86	82	8	0	89	81	180	CMT
7	12/ 3/85	26.96N	140.35E	425.4	6.1	86	489	0.64	75	70	23	16	129	68	356	CMT
8	11/17/84	28.29N	139.85E	439.7	5.3	83	496	0.86	82	86	7	6	175	84	324	CMT
9	5/13/77	28.42N	139.50E	439.7	5.8	78	504	0.67	75	75	20	25	60	60	275	CMT
10	9/ 8/82	27.12N	140.11E	441.4	5.4	83	496	0.38	72	55	40	11	252	52	357	CMT
11	4/ 3/85	28.29N	139.33E	455.1	5.9	75	516	0.69	77	73	21	24	36	55	265	CMT
12	3/17/86	27.37N	139.83E	457.7	5.5	74	527	0.66	81	63	27	7	61	60	318	CMT
13	10/ 4/85	27.63N	139.90E	467.7	5.6	75	536	0.86	87	71	18	16	49	61	287	CMT
14	7/11/51	28.10N	139.90E	475.0	—	74	525	0.67	77	71	22	26	37	53	268	RA
15	5/10/78	27.80N	139.73E	493.8	5.0	78	556	0.74	79	75	18	18	19	60	255	CMT
16	9/10/85	27.21N	139.81E	496.9	5.8	76	566	0.77	80	76	16	21	35	60	263	CMT
17	5/21/84	27.34N	139.83E	504.9	5.0	76	566	0.53	67	83	23	35	42	55	223	CMT
18	1/17/80	28.31N	138.83E	507.0	5.3	25	621	0.56	69	82	22	84	38	5	241	CMT
19	3/ 3/65	28.12N	139.51E	507.0	—	76	565	0.68	78	85	28	20	18	48	255	OI
20	9/ 5/85	28.04N	139.34E	515.5	4.9	57	584	0.72	79	72	20	2	324	76	228	CMT
21	2/ 3/86	27.89N	139.40E	516.0	5.7	44	594	0.87	83	85	7	28	1	38	247	CMT
22	10/14/82	27.49N	139.84E	517.1	5.1	70	573	0.75	80	75	18	20	8	70	196	CMT
N16	θ_s=247.9	$\overline{\delta_s}$=94														
1	3/15/78	26.42N	140.56E	270.1	6.1	89	249	0.08	67	39	59	23	70	30	326	CMT
2	12/11/80	26.53N	140.53E	475.9	5.3	98	445	0.82	82	78	14	1	256	77	350	CMT
N17	θ_s=248.3	$\overline{\delta_s}$=85														
1	2/28/86	23.75N	141.75E	87.7	5.1	61	85	-0.03	74	18	81	23	148	19	50	CMT
2	5/29/87	22.47N	143.18E	133.7	5.2	62	95	-0.31	32	84	58	46	198	37	340	CMT
3	7/ 7/85	22.63N	141.96E	252.6	5.4	88	249	0.84	84	76	15	7	103	73	218	CMT
4	2/ 8/80	22.40N	142.02E	278.9	5.3	89	274	0.01	50	65	49	40	43	40	179	CMT
5	5/25/79	24.11N	142.24E	578.7	5.5	94	568	0.42	63	77	29	29	193	56	46	CMT
6	5/18/79	24.13N	142.40E	580.9	5.8	94	567	0.94	87	83	7	2	149	87	285	CMT
N18	θ_s=249.7	$\overline{\delta_s}$=60														
1	12/ 4/84	22.61N	143.25E	100.0	5.8	52	114	0.25	60	66	39	27	174	59	322	CMT
2	2/27/82	22.26N	143.53E	103.6	5.9	52	115	0.12	78	28	63	25	52	14	315	CMT
3	11/29/79	22.44N	143.31E	113.3	5.3	52	113	-0.12	41	76	51	32	199	19	301	CMT
4	3/12/84	22.21N	143.16E	191.7	5.3	64	192	-0.22	52	42	74	62	91	14	332	CMT
5	7/27/77	21.65N	142.95E	296.0	5.1	81	326	-0.98	5	84	89	77	266	5	18	CMT
N19	θ_s=252.1	$\overline{\delta_s}$=79														
1	1/21/87	20.61N	144.83E	113.3	5.6	57	125	0.79	78	89	11	43	88	46	255	CMT
2	7/24/77	19.50N	144.72E	409.1	5.4	76	416	0.63	72	80	19	5	230	74	338	CMT
3	12/27/86	19.91N	144.27E	425.9	5.1	78	437	0.30	63	64	38	20	201	47	314	CMT
4	8/15/78	19.73N	144.40E	488.9	5.4	83	498	0.72	76	83	15	17	134	73	317	CMT
5	12/27/82	19.01N	145.01E	608.8	5.3	88	605	0.68	75	78	18	16	32	70	249	CMT
6	3/ 7/62	19.10N	145.20E	683.0	—	90	688	0.99	89	89	0	0	49	90	49	KS
N20	θ_s=258.7	$\overline{\delta_s}$=73														
1	6/17/77	19.04N	145.69E	82.7	5.6	54	115	-0.08	61	36	70	21	189	15	93	CMT
2	10/19/78	17.04N	146.00E	99.1	5.3	53	104	-0.35	46	45	78	37	194	46	54	CMT
3	5/ 2/85	19.19N	145.76E	113.4	5.1	53	103	-0.05	67	28	73	21	179	52	60	CMT

Table 1. (*continued*)

	Event Information					Slab			Angle from down-dip			T Axis		P Axis		
	Date	Lat. (°)	Lon. (°)	Depth (km)	m_b	δ_s (°)	L (km)	κ	η_T (°)	η_B (°)	η_P (°)	δ (°)	θ (°)	δ (°)	θ (°)	Ref.
4	1/ 2/65	19.10N	145.80E	136.0	—	55	125	0.06	67	37	61	22	177	60	43	KS
5	5/ 9/87	19.13N	145.62E	144.4	5.2	59	154	-0.00	86	4	87	2	158	28	67	CMT
6	9/14/83	18.09N	145.81E	148.4	6.0	59	152	-0.05	70	23	78	12	187	42	85	CMT
7	4/ 7/82	18.93N	145.42E	157.0	—	59	165	-0.20	53	42	72	28	194	48	68	CMT
8	9/ 9/78	18.55N	145.50E	193.0	5.2	68	206	-0.74	27	62	87	56	202	19	82	CMT
9	12/18/78	18.57N	145.54E	200.9	5.2	69	215	-0.40	45	44	82	46	174	13	69	CMT
10	10/14/81	18.48N	145.73E	202.5	5.0	69	222	-0.66	26	64	80	55	207	29	65	CMT
11	5/25/85	17.57N	145.60E	205.6	5.3	69	215	-0.13	54	46	66	47	144	33	9	CMT
12	5/24/77	18.81N	145.35E	206.1	5.7	69	216	-0.28	49	44	75	47	161	6	64	CMT
13	4/14/85	18.66N	145.51E	214.4	5.0	69	226	-0.21	57	33	80	41	151	9	54	CMT
14	5/13/79	19.00N	145.34E	215.6	5.9	69	223	-0.25	50	43	75	48	152	4	58	CMT
15	4/13/86	17.19N	145.62E	296.7	5.1	77	307	-0.94	10	79	88	71	230	9	111	CMT
16	12/25/79	18.74N	145.25E	576.0	5.4	90	588	0.27	74	44	49	15	58	41	314	CMT
17	10/30/79	18.79N	145.13E	578.7	5.6	90	588	0.56	72	70	26	17	89	64	322	CMT
18	10/17/79	18.52N	145.28E	583.8	6.1	90	596	0.66	89	55	34	0	260	55	350	CMT
19	5/10/70	18.62N	145.41E	587.0	—	90	599	0.79	86	67	23	4	261	66	4	ST
20	2/27/77	18.65N	145.29E	592.6	5.0	91	605	0.67	84	59	30	4	75	60	337	CMT
21	1/ 4/82	18.03N	145.63E	595.2	6.1	91	607	0.77	78	89	11	13	256	77	78	CMT
N21	θ_s=277.7	$\overline{\delta_s}$=83														
1	4/17/87	15.35N	145.80E	94.9	5.3	51	73	-0.71	23	68	80	37	303	47	87	CMT
2	11/ 7/77	15.28N	144.98E	263.8	5.4	79	266	0.49	80	52	38	18	133	54	17	CMT
3	6/ 7/81	16.59N	145.47E	311.8	5.7	86	305	-0.79	14	80	80	73	247	10	15	CMT
T1	θ_s=258.0	$\overline{\delta_s}$=48														
1	6/18/80	15.27S	173.57W	72.8	5.9	34	71	-0.04	56	37	77	46	183	36	45	CMT
2	4/13/86	15.47S	173.35W	73.4	5.3	25	24	0.18	63	43	57	29	185	32	75	CMT
3	9/11/85	15.38S	173.60W	76.6	5.7	34	68	-0.34	26	66	77	59	274	26	129	CMT
4	11/14/78	15.66S	173.23W	76.2	5.4	32	60	-0.26	28	66	73	53	230	37	51	CMT
5	9/15/80	15.65S	173.74W	80.6	5.3	37	84	-0.05	41	78	50	41	203	23	315	CMT
6	4/15/86	15.46S	174.05W	84.4	5.3	47	102	0.84	75	82	17	53	113	35	274	CMT
7	4/27/85	15.32S	173.57W	90.4	5.7	34	73	-0.60	13	79	81	48	259	25	136	CMT
8	3/23/79	15.21S	174.06W	97.9	5.2	53	122	0.86	77	88	11	27	151	48	274	CMT
9	11/29/86	16.39S	173.86W	100.5	5.3	53	120	0.07	54	45	66	70	114	16	330	CMT
10	3/11/68	16.20S	173.90W	112.0	6.2	53	135	0.16	76	55	37	19	49	63	184	IM
11	10/15/84	15.74S	173.79W	119.7	6.5	47	103	-0.66	7	83	86	42	265	44	56	CMT
12	12/23/81	15.36S	173.80W	119.6	5.6	51	113	-0.47	17	73	86	48	232	41	61	CMT
13	10/19/84	15.86S	174.00W	124.5	5.7	53	124	-0.52	7	82	87	51	270	39	91	CMT
14	10/26/69	16.20S	173.90W	127.0	—	53	145	-0.64	8	82	84	55	243	26	110	Ri
15	11/26/77	15.27S	174.40W	157.9	5.3	58	182	0.84	89	88	1	6	359	58	260	CMT
16	4/18/84	15.94S	174.35W	158.0	5.9	58	182	0.50	84	85	7	24	97	65	264	CMT
17	1/22/80	16.00S	174.15W	173.1	5.3	58	191	-0.70	4	86	87	55	264	34	69	CMT
18	11/30/85	16.38S	174.20W	179.1	5.6	58	205	-0.37	32	59	80	52	201	22	81	CMT
19	4/26/80	15.59S	174.34W	185.2	5.5	57	214	-0.69	28	82	63	29	256	58	103	CMT
20	8/13/81	16.05S	174.41W	188.0	5.4	57	215	-0.43	32	62	73	64	190	26	358	CMT
21	8/ 9/85	15.34S	174.65W	221.3	5.4	54	255	0.41	74	66	29	18	60	68	201	CMT
22	6/ 4/74	15.89S	175.04W	256.0	6.3	56	321	-0.63	25	74	71	39	286	50	106	Ri
23	11/ 5/85	16.45S	177.27W	266.7	5.3	31	572	-0.31	36	68	62	33	302	39	180	CMT
24	6/15/84	15.79S	174.87W	269.6	6.2	55	305	0.65	76	88	13	17	105	66	240	CMT
25	5/29/83	15.58S	174.98W	275.6	5.5	56	315	0.55	78	67	24	17	111	72	305	CMT
26	7/ 3/80	15.14S	174.98W	283.6	5.0	56	315	0.51	72	76	22	16	84	71	297	CMT
27	7/12/80	15.78S	175.09W	287.5	5.3	51	344	0.55	76	57	35	23	97	59	321	CMT
28	6/10/84	15.88S	175.03W	308.1	4.9	47	353	0.05	48	65	50	29	317	57	170	CMT
29	8/ 9/78	14.88S	176.09W	315.9	5.2	30	453	0.14	74	26	69	43	63	25	178	CMT
30	6/ 5/85	14.97S	177.67W	380.3	5.1	31	623	-0.26	46	56	62	5	298	85	118	CMT
31	11/18/78	16.76S	176.91W	410.2	5.3	31	574	0.45	89	42	47	54	110	9	213	CMT
32	12/15/86	15.74S	177.72W	429.1	5.0	31	612	0.76	89	63	27	49	121	17	233	CMT
33	9/ 6/86	15.56S	178.09W	435.8	5.0	36	653	0.02	61	36	68	79	27	10	187	CMT
34	6/19/85	15.97S	178.10W	473.1	4.9	38	690	0.78	81	54	36	42	141	7	237	CMT
35	12/25/80	16.58S	178.91W	502.1	5.0	43	779	-0.08	45	48	74	30	202	30	92	CMT
36	4/13/87	16.82S	179.37W	530.6	5.0	43	802	-0.08	69	22	81	10	127	26	32	CMT
37	8/ 1/86	16.91S	179.06W	531.3	4.9	43	804	0.37	81	38	52	18	137	1	46	CMT
38	11/16/85	17.53S	178.93W	568.6	5.1	43	812	0.30	69	88	21	9	128	51	229	CMT
T2	θ_s=262.5	$\overline{\delta_s}$=56														
1	8/20/86	16.87S	173.65W	75.9	5.5	32	28	-0.84	19	70	87	27	241	60	90	CMT
2	4/27/82	16.54S	174.17W	91.3	—	39	114	0.85	89	67	22	47	57	30	288	CMT
3	8/11/77	17.56S	174.37W	106.0	6.3	39	134	0.80	79	86	10	39	71	49	270	CMT
4	6/11/82	17.53S	174.46W	113.2	6.3	39	133	0.74	76	88	13	34	105	53	259	CMT

Table 1. (*continued*)

	Event Information					Slab			Angle from down-dip			T Axis		P Axis		
	Date	Lat. (°)	Lon. (°)	Depth (km)	m_b	δ_s (°)	L (km)	κ	η_T (°)	η_B (°)	η_P (°)	δ (°)	θ (°)	δ (°)	θ (°)	Ref.
5	2/ 1/85	17.62S	174.49W	127.3	5.6	39	138	0.79	80	77	15	37	110	52	277	CMT
6	10/17/86	16.23S	174.08W	129.8	5.3	32	44	-0.64	21	75	74	39	237	38	108	CMT
7	5/28/81	17.08S	173.98W	131.2	5.4	40	152	-0.20	57	33	80	27	332	39	86	CMT
8	4/25/86	17.20S	174.15W	139.6	5.3	39	129	-0.77	12	84	78	52	269	38	90	CMT
9	7/28/84	17.07S	174.07W	144.2	5.5	39	134	-0.63	26	67	78	55	230	35	59	CMT
10	10/30/84	17.12S	174.11W	150.3	6.0	39	124	-0.75	14	80	78	53	273	36	103	CMT
11	1/17/75	17.90S	174.60W	153.0	5.8	48	202	0.59	70	83	21	11	124	67	241	Ri
12	6/25/78	17.11S	174.43W	163.7	5.5	45	174	0.60	75	68	26	18	175	61	300	CMT
13	8/15/83	17.10S	174.59W	180.7	5.5	48	219	0.44	71	62	35	16	117	73	320	CMT
14	6/ 1/83	17.00S	174.71W	185.7	6.1	48	203	0.59	79	60	31	21	126	68	313	CMT
15	7/30/86	18.01S	174.91W	196.8	4.8	41	280	-0.00	85	4	88	22	21	36	129	CMT
16	5/ 1/69	16.70S	174.60W	205.0	6.1	48	225	0.14	84	25	65	13	16	59	131	Ri
17	5/22/72	17.70S	175.20W	227.0	6.1	41	294	0.08	56	71	50	9	210	80	3	Ri
18	10/13/84	17.76S	175.19W	250.9	5.2	41	284	0.68	79	69	23	30	118	60	288	CMT
19	10/28/79	16.65S	174.78W	265.3	5.0	41	273	0.44	76	53	39	39	12	50	206	CMT
20	2/25/84	16.69S	174.82W	269.0	5.7	41	273	0.23	65	53	45	36	351	52	195	CMT
21	6/15/84	17.98S	175.16W	271.7	5.1	43	312	-0.05	57	43	63	30	335	20	78	CMT
22	4/26/87	17.17S	175.08W	277.4	5.4	41	284	0.68	85	60	30	1	0	72	268	CMT
23	5/28/79	17.55S	175.20W	286.0	5.3	46	344	0.82	84	86	6	35	106	50	254	CMT
24	7/31/84	17.59S	175.76W	297.8	5.1	45	405	0.91	85	89	4	39	68	50	263	CMT
25	4/25/84	17.29S	177.23W	418.4	5.7	52	574	0.91	81	88	8	42	116	44	265	CMT
26	9/ 1/84	18.14S	178.21W	485.7	5.4	62	695	-0.03	51	65	49	18	225	34	328	CMT
27	1/16/86	17.52S	178.90W	509.7	5.1	63	705	0.03	47	66	50	37	331	19	226	CMT
28	2/25/80	17.69S	178.50W	529.4	5.5	58	752	-0.03	58	43	63	35	177	5	84	CMT
29	4/14/77	17.67S	178.65W	533.4	5.2	58	774	0.43	75	55	39	14	177	75	11	CMT
30	7/ 3/84	17.68S	178.89W	533.4	5.7	58	775	-0.27	35	81	57	60	334	6	232	CMT
31	4/10/65	17.80S	178.80W	535.0	—	58	765	0.32	60	74	35	33	348	28	236	ISO
32	7/17/87	17.90S	179.27E	537.9	—	58	795	0.83	89	65	24	19	25	37	280	CMT
33	1/20/84	17.78S	178.59W	545.2	5.3	58	772	-0.26	34	87	55	71	181	8	295	CMT
34	11/27/86	18.11S	178.48W	547.5	5.1	58	752	0.52	73	62	33	27	160	25	264	CMT
35	8/29/79	17.62S	178.89W	551.2	5.3	58	794	0.01	54	54	55	39	347	4	254	CMT
36	7/24/79	17.54S	178.88W	556.2	5.2	58	794	0.63	80	62	29	2	337	32	245	CMT
37	9/25/82	17.58S	179.08W	556.8	—	58	795	0.44	63	83	26	7	213	69	322	CMT
38	12/27/77	17.97S	178.63W	557.0	5.3	58	785	-0.52	37	54	81	83	40	5	180	CMT
39	7/29/86	17.55S	178.58W	559.7	5.1	58	773	0.38	66	65	34	5	57	49	321	CMT
40	1/17/82	17.76S	179.04W	560.9	—	60	801	-0.52	22	86	68	64	310	1	218	CMT
41	9/30/84	17.70S	178.79W	560.5	4.8	58	793	0.00	45	79	46	53	349	17	235	CMT
42	6/14/80	18.28S	177.97W	561.0	5.6	59	745	0.29	61	64	39	47	145	43	323	CMT
43	4/ 1/86	17.91S	178.63W	562.4	5.7	58	774	-0.27	37	72	58	23	244	63	97	CMT
44	8/25/63	17.50S	178.70W	563.0	—	58	781	0.80	84	71	19	33	118	42	244	ISO
45	7/29/79	17.70S	178.55W	566.5	5.4	58	784	0.63	70	86	18	49	108	41	274	CMT
46	4/ 6/85	17.80S	178.71W	567.6	5.2	58	772	0.91	89	72	17	15	18	42	274	CMT
47	10/16/78	17.75S	178.82W	568.8	5.4	60	803	-0.42	26	85	64	69	323	0	233	CMT
48	3/ 8/77	17.84S	178.71W	574.4	5.3	58	795	0.53	67	83	24	32	1	39	240	CMT
49	8/23/79	17.81S	178.78W	576.5	5.3	62	815	0.12	50	74	43	48	357	21	241	CMT
50	2/14/87	17.83S	178.72W	577.9	5.7	60	805	0.02	49	65	51	53	0	9	258	CMT
51	10/27/85	17.67S	178.89W	577.0	5.2	58	795	0.20	57	65	42	60	123	18	246	CMT
52	3/15/86	17.41S	178.99W	577.6	5.2	60	801	0.14	72	35	59	5	326	4	236	CMT
53	12/12/86	17.88S	178.69W	579.1	5.2	62	815	0.65	73	88	16	5	42	69	299	CMT
54	11/ 9/79	17.75S	178.72W	588.0	5.5	62	815	0.51	64	86	25	49	43	37	252	CMT
55	7/21/66	17.80S	178.60W	590.0	5.8	58	795	-0.04	76	14	86	6	189	27	95	ISO
56	1/31/87	17.97S	178.50W	592.2	5.2	62	815	-0.02	46	70	50	52	353	13	246	CMT
57	9/12/64	17.60S	179.70W	592.0	—	64	855	0.59	70	86	19	41	44	48	243	ISO
58	8/13/78	17.81S	178.35W	593.5	5.5	58	791	0.35	66	63	36	8	88	63	342	CMT
59	4/27/86	17.87S	178.43W	594.4	5.2	58	791	0.91	87	82	8	26	108	64	277	CMT
60	11/ 6/86	17.96S	178.47W	597.1	5.4	58	795	0.89	83	87	7	17	9	59	249	CMT
61	3/ 3/83	17.84S	178.37W	597.4	—	58	791	0.29	60	72	34	2	79	68	344	CMT
62	5/25/77	17.86S	178.62W	598.3	5.4	63	824	0.55	76	58	35	19	0	28	259	CMT
63	8/ 7/86	17.99S	178.42W	603.4	5.0	58	785	0.87	89	69	20	14	18	40	276	CMT
64	1/10/84	17.60S	178.61W	603.8	5.1	62	812	0.20	85	32	57	22	102	38	354	CMT
65	5/17/78	17.98S	178.42W	604.7	5.1	62	813	-0.37	31	68	67	63	335	5	75	CMT
66	11/23/83	17.98S	178.52W	605.8	—	60	805	-0.55	28	70	71	49	309	41	132	CMT
67	1/21/77	18.01S	178.38W	607.0	5.8	58	795	0.91	86	85	5	27	67	63	255	CMT
68	7/20/80	17.87S	178.63W	608.0	6.0	63	823	0.67	77	64	28	27	22	35	271	CMT
69	1/ 1/82	17.94S	178.49W	609.8	5.5	60	805	0.60	75	65	28	33	25	32	272	CMT
70	5/15/87	17.89S	178.64W	610.0	4.9	64	835	-0.18	39	77	53	47	329	20	216	CMT
71	8/30/81	17.97S	178.50W	618.4	5.4	60	805	-0.17	40	67	58	60	351	2	257	CMT
72	3/29/86	17.87S	178.69W	618.3	5.3	63	825	0.15	57	59	47	32	342	18	240	CMT
73	12/ 4/80	17.79S	179.96W	619.4	5.1	69	884	0.51	66	81	25	22	344	52	222	CMT
74	5/17/87	18.00S	178.61W	619.3	5.3	62	814	0.06	56	50	57	48	13	6	277	CMT

Table 1. (*continued*)

	Event Information					Slab			Angle from down-dip			T Axis		P Axis		
	Date	Lat. (°)	Lon. (°)	Depth (km)	m_b	δ_s (°)	L (km)	κ	η_T (°)	η_B (°)	η_P (°)	δ (°)	θ (°)	δ (°)	θ (°)	Ref.
75	8/11/87	17.94S	178.60W	621.5	—	63	825	0.16	67	41	57	45	45	13	302	CMT
76	4/12/79	18.03S	178.14W	622.8	5.4	60	805	0.79	89	65	25	27	114	61	315	CMT
77	8/ 6/87	18.30S	178.51W	623.8	—	62	815	0.65	73	74	22	44	97	46	290	CMT
78	12/25/65	18.20S	179.10W	624.0	—	64	853	0.98	88	88	2	3	2	67	264	ISO
79	10/18/77	18.04S	178.41W	629.4	5.3	63	824	0.52	66	74	28	40	23	35	257	CMT
80	1/25/86	18.11S	177.81W	634.9	4.9	58	783	0.00	51	60	51	59	149	31	329	CMT
81	1/28/82	17.85S	179.40W	639.2	5.4	69	886	0.44	59	89	30	48	45	40	246	CMT
82	7/29/87	18.20S	178.35W	645.3	—	64	833	0.72	75	87	14	11	343	59	233	CMT
83	12/ 9/65	18.12S	178.12W	649.0	5.7	63	824	0.16	85	72	70	3	8	46	94	ISO
84	7/29/87	18.05S	178.33W	654.0	—	64	835	0.80	81	78	13	5	343	53	246	CMT
85	10/20/81	18.14S	179.40W	656.0	5.6	69	903	0.24	50	84	39	58	54	32	241	CMT
86	11/22/84	17.77S	178.09W	663.0	5.8	64	833	0.08	68	37	60	2	222	14	312	CMT
T3	θ_s=270.0	$\bar{\delta}_s$=58														
1	7/30/82	18.63S	173.87W	70.3	5.5	24	107	-0.53	15	84	75	36	258	47	116	CMT
2	4/17/87	20.32S	174.36W	87.4	5.3	27	154	0.90	80	77	15	59	150	13	263	CMT
3	8/10/66	20.20S	175.30W	95.0	—	39	243	0.68	73	89	16	29	62	54	282	ISO
4	3/26/77	18.59S	174.15W	105.2	5.6	28	160	-0.19	32	79	59	47	304	28	69	CMT
5	1/15/72	18.30S	174.60W	155.0	—	33	223	0.80	81	89	11	43	123	37	257	Bi
6	11/14/69	19.70S	175.80W	209.0	—	47	355	0.82	81	89	13	34	91	54	251	Bi
7	4/18/83	19.70S	175.70W	214.6	—	47	354	0.15	73	37	57	23	113	17	210	CMT
8	10/14/79	20.19S	175.93W	216.5	5.4	47	355	0.59	75	67	26	23	120	42	233	CMT
9	3/21/82	18.51S	175.27W	217.3	5.8	46	323	0.74	76	86	13	27	115	60	267	CMT
10	3/18/65	19.90S	175.90W	219.0	6.0	47	370	0.09	84	74	80	37	140	32	79	ISO
11	6/28/86	19.99S	176.08W	222.1	6.1	47	355	0.97	89	80	9	40	114	44	258	CMT
12	12/27/71	19.90S	175.80W	224.0	—	47	364	0.89	85	89	16	22	162	32	267	Bi
13	7/10/86	19.92S	175.77W	226.2	5.2	47	363	0.75	76	86	13	46	139	38	283	CMT
14	4/15/83	19.10S	175.61W	226.0	5.7	47	355	0.83	81	87	8	19	142	55	262	CMT
15	3/ 4/67	18.40S	175.40W	228.0	—	47	342	0.90	86	89	18	32	144	32	258	Bi
16	4/29/84	19.91S	175.56W	229.5	5.4	47	361	0.76	82	70	20	19	144	35	248	CMT
17	4/28/79	19.35S	175.66W	229.7	5.3	47	364	0.81	86	69	21	39	88	46	301	CMT
18	11/18/84	18.72S	175.60W	229.7	5.6	47	332	0.72	77	77	17	19	135	44	245	CMT
19	11/30/80	19.43S	175.85W	238.0	6.0	47	400	0.88	85	75	15	43	123	46	292	CMT
20	1/18/87	19.53S	175.65W	245.6	5.1	47	371	0.73	77	78	18	47	136	30	266	CMT
21	11/ 6/84	18.64S	175.48W	246.7	5.4	47	353	0.93	87	82	7	34	124	53	279	CMT
22	9/17/87	18.48S	175.30W	246.1	—	47	345	0.87	83	81	10	37	141	48	286	CMT
23	6/ 6/77	19.24S	175.64W	247.2	5.1	47	369	0.42	81	47	44	51	87	26	320	CMT
24	9/15/85	19.11S	175.81W	258.0	5.7	47	379	0.83	82	83	10	27	130	58	272	CMT
25	2/ 4/86	19.47S	175.76W	268.1	5.2	47	365	0.92	89	76	13	26	146	57	286	CMT
26	12/14/86	18.04S	175.01W	273.3	5.0	47	341	0.09	57	56	50	60	18	0	108	CMT
27	1/22/87	19.00S	175.70W	278.4	5.1	47	393	0.53	65	84	24	65	116	25	282	CMT
28	1/ 6/83	19.93S	176.20W	280.1	—	47	433	-0.14	46	63	55	4	250	33	343	CMT
29	11/15/84	20.36S	177.46W	305.3	5.7	63	552	-0.34	40	65	60	23	260	38	9	CMT
30	5/22/77	19.52S	177.25W	346.9	5.2	63	555	0.09	72	37	58	8	71	24	338	CMT
31	5/21/62	19.90S	177.20W	351.0	—	63	553	0.84	78	76	18	38	98	50	294	IM
32	1/14/77	19.80S	177.54W	358.2	5.2	64	585	-0.37	37	72	58	29	250	39	8	CMT
33	7/ 7/83	19.00S	177.47W	378.6	—	66	594	-0.37	46	49	71	23	245	11	339	CMT
34	4/29/87	18.93S	177.86W	410.6	5.9	69	636	-0.12	35	80	55	54	195	22	318	CMT
35	2/10/87	19.45S	177.48W	418.5	6.1	68	624	0.86	84	79	12	27	94	61	294	CMT
36	11/18/65	18.80S	177.80W	424.0	6.2	71	645	0.40	57	75	38	37	173	37	300	ISO
37	11/17/84	18.74S	178.09W	471.5	6.0	77	693	-0.18	31	80	60	64	163	26	339	CMT
38	10/10/85	18.61S	178.07W	495.4	4.9	84	714	0.38	44	88	44	49	141	41	309	CMT
39	5/15/77	19.13S	177.67W	506.4	5.5	84	717	0.82	76	87	13	19	93	71	278	CMT
40	2/23/85	18.33S	178.12W	526.1	5.1	85	738	0.63	66	81	25	26	147	63	338	CMT
41	11/29/83	19.49S	177.81W	540.0	5.8	83	757	0.03	69	78	24	14	273	71	49	CMT
42	7/27/80	19.65S	179.93E	553.5	5.3	—	—	—	—	—	—	13	265	11	358	CMT
43	4/22/77	17.75S	178.28W	554.3	5.5	83	766	0.86	69	70	29	24	150	54	277	CMT
44	12/30/86	18.88S	177.91W	563.2	5.2	82	778	0.01	79	49	42	6	315	53	54	CMT
45	6/ 3/77	18.94S	177.63W	565.5	5.3	82	775	0.09	59	75	34	27	216	55	352	CMT
46	10/ 5/77	18.58S	177.72W	575.2	5.6	80	787	0.84	78	87	11	21	108	69	285	CMT
47	5/25/83	18.66S	177.60W	581.5	—	80	788	0.58	85	79	11	4	58	74	314	CMT
48	5/ 1/78	19.25S	177.50W	584.7	5.5	80	785	0.82	82	73	18	15	127	63	249	CMT
49	4/22/80	18.18S	178.11W	595.9	5.6	56	833	0.35	71	54	41	37	154	52	345	CMT
50	8/ 7/85	19.40S	178.30W	643.4	5.3	56	842	0.36	75	50	43	6	198	16	289	CMT
51	12/ 8/83	19.07S	178.52W	649.3	5.4	51	871	0.77	83	71	19	3	186	33	278	CMT
T4	θ_s=278.5	$\bar{\delta}_s$=60														
1	7/29/86	21.31S	175.54W	137.1	5.4	50	182	0.56	68	87	21	18	103	71	265	CMT
2	8/26/87	21.14S	175.53W	141.7	—	48	169	-0.69	15	83	75	59	258	25	115	CMT
3	6/16/81	20.31S	175.26W	164.3	5.4	50	184	-0.39	50	39	89	29	341	39	97	CMT

Table 1. (*continued*)

	Event Information					Slab			Angle from down-dip			T Axis		P Axis		
	Date	Lat. (°)	Lon. (°)	Depth (km)	m_b	δ_s (°)	L (km)	κ	η_T (°)	η_B (°)	η_P (°)	δ (°)	θ (°)	δ (°)	θ (°)	Ref
4	10/12/85	21.62S	176.49W	170.1	5.8	51	214	0.87	83	82	9	31	118	54	263	CMT
5	10/30/86	21.69S	176.68W	196.3	6.4	55	261	0.89	84	84	7	40	111	50	288	CMT
6	4/10/82	18.93N	145.42E	198.1	—	55	262	0.69	73	88	15	50	114	40	283	CMT
7	3/19/87	20.32S	176.27W	215.3	5.8	55	261	0.88	83	83	8	38	126	47	273	CMT
8	11/11/79	20.26S	176.15W	218.0	5.5	55	275	0.97	88	88	2	35	118	54	282	CMT
9	3/ 2/84	20.98S	176.71W	231.3	5.4	54	294	0.75	77	87	13	21	120	67	274	CMT
10	6/21/81	20.79S	176.30W	235.2	5.3	53	304	0.13	74	34	60	52	105	16	217	CMT
11	12/19/73	20.60S	176.50W	246.0	—	52	315	0.78	78	84	12	43	138	42	288	Ri
12	9/26/68	20.90S	176.70W	251.0	6.0	51	331	0.10	63	69	56	13	341	71	118	Ri
13	2/18/70	20.80S	176.90W	259.0	—	52	351	0.62	85	84	45	41	112	38	342	Ri
14	4/27/85	20.93S	176.99W	261.8	5.7	51	342	0.05	87	14	75	40	105	14	3	CMT
15	5/ 3/78	21.40S	177.40W	302.8	5.4	56	425	0.42	86	42	47	29	84	30	335	CMT
16	2/18/79	20.58S	177.83W	378.1	5.1	70	502	-0.50	30	67	70	43	252	17	358	CMT
17	11/ 6/83	20.13S	177.69W	393.8	5.5	72	512	0.07	62	46	55	45	99	27	339	CMT
18	10/19/78	21.24S	177.82W	396.8	5.3	67	495	0.65	72	77	21	5	111	81	350	CMT
19	6/16/81	20.06S	177.73W	408.3	5.0	72	526	0.51	78	59	32	29	91	47	324	CMT
20	6/ 3/86	20.66S	178.06W	504.7	5.4	74	616	0.81	82	76	15	21	68	60	296	CMT
21	4/14/86	20.44S	177.81W	509.0	5.3	74	607	0.69	74	86	16	14	0	66	236	CMT
22	11/13/81	20.60S	177.87W	512.9	5.5	74	626	0.74	78	78	16	27	94	60	302	CMT
23	5/ 3/78	20.26S	177.90W	515.8	5.2	74	627	-0.04	54	52	57	41	24	17	278	CMT
24	10/ 7/78	20.19S	177.68W	522.7	5.1	74	625	0.86	86	74	15	4	159	61	256	CMT
25	11/21/85	20.74S	178.16W	528.6	5.4	71	645	0.52	66	89	23	39	136	49	296	CMT
26	1/ 7/86	21.11S	178.75W	531.5	5.2	71	645	0.78	84	73	17	2	199	87	336	CMT
27	2/ 5/85	20.57S	177.75W	533.2	5.3	73	636	0.70	78	73	21	13	12	53	263	CMT
28	4/10/71	21.20S	178.80W	533.0	—	63	672	0.48	67	86	30	12	216	76	12	Bi
29	11/30/82	20.44S	178.05W	539.1	5.2	64	664	0.62	75	70	25	9	121	76	354	CMT
30	3/15/85	20.63S	178.33W	539.9	5.5	64	663	0.64	78	67	25	8	61	51	321	CMT
31	5/22/65	21.10S	178.60W	540.0	—	64	665	0.53	69	78	24	14	208	71	347	ISO
32	7/ 1/83	20.78S	178.60W	544.1	—	63	675	0.78	83	73	20	30	130	56	317	CMT
33	10/17/78	20.63S	178.16W	547.0	5.4	64	666	0.71	85	62	27	14	55	44	312	CMT
34	11/ 9/82	21.38S	178.73W	554.4	5.2	61	704	0.72	84	64	26	29	135	60	334	CMT
35	10/ 3/80	20.21S	177.78W	558.8	5.4	63	675	0.79	83	71	18	12	18	45	276	CMT
36	11/30/77	20.61S	178.42W	559.8	5.5	63	695	0.62	72	78	21	30	167	57	320	CMT
37	3/22/80	20.67S	178.25W	560.3	5.0	63	672	0.69	75	80	16	10	201	53	304	CMT
38	8/11/79	20.61S	178.36W	561.7	5.3	63	685	0.64	85	57	32	18	161	70	8	CMT
39	12/ 5/85	20.56S	178.43W	561.5	4.9	63	685	0.87	82	86	7	15	65	71	281	CMT
40	1/ 5/77	20.81S	178.31W	561.8	5.2	63	694	0.71	76	83	16	25	169	58	310	CMT
41	7/16/82	21.40S	178.93W	562.0	5.6	58	722	0.42	62	88	27	16	216	56	331	CMT
42	5/26/86	20.07S	178.72E	567.5	6.8	—	—	—	—	—	—	40	174	43	34	CMT
43	5/11/87	20.43S	178.53W	568.6	5.3	61	703	0.55	70	74	24	40	149	50	318	CMT
44	7/20/79	20.47S	178.37W	570.2	5.4	63	695	0.74	78	75	19	38	87	47	299	CMT
45	7/20/84	20.82S	178.43W	574.6	5.2	59	715	0.86	85	76	14	1	20	74	288	CMT
46	6/ 5/86	20.07S	178.74E	574.2	5.1	—	—	—	—	—	—	4	345	9	254	CMT
47	11/27/77	20.48S	178.43W	575.4	5.6	61	702	0.53	68	79	23	39	159	49	315	CMT
48	3/14/84	20.04S	178.11W	576.1	5.7	63	684	0.42	68	66	33	45	129	43	326	CMT
49	8/10/77	20.73S	178.45W	577.0	5.4	59	715	0.84	88	68	21	26	126	62	324	CMT
50	6/28/79	20.24S	178.20W	578.6	5.3	63	695	0.98	89	88	2	24	132	61	277	CMT
51	3/14/77	20.73S	178.51W	579.0	5.4	58	721	0.89	84	82	9	1	197	51	288	CMT
52	4/16/77	21.49S	179.21W	581.8	5.2	57	745	0.12	56	61	47	31	203	59	17	CMT
53	8/26/87	20.80S	178.60W	588.3	—	59	715	0.67	81	65	26	39	103	45	316	CMT
54	5/ 3/87	20.79S	178.66W	591.4	5.3	58	725	0.64	72	84	18	5	214	53	311	CMT
55	3/31/81	21.05S	178.82W	591.7	5.2	58	762	0.98	89	86	3	3	185	62	280	CMT
56	10/ 2/80	20.97S	178.67W	592.3	5.3	57	745	0.83	82	79	13	19	61	55	302	CMT
57	9/15/84	20.75S	178.50W	592.6	5.5	58	725	0.23	55	75	37	7	249	54	348	CMT
58	5/ 3/83	20.21S	178.49W	592.1	—	59	715	0.63	71	84	19	3	220	57	315	CMT
59	10/20/84	20.65S	178.51W	593.7	5.4	59	711	0.54	68	83	22	46	144	42	302	CMT
60	9/ 6/86	20.64S	178.55W	593.2	5.2	58	725	0.90	86	77	12	35	111	55	301	CMT
61	10/30/77	20.42S	178.57W	595.4	5.6	58	725	0.46	63	88	25	26	197	46	316	CMT
62	7/ 6/77	21.07S	178.57W	596.2	5.8	58	725	0.48	75	58	34	17	94	52	341	CMT
63	11/ 6/79	21.08S	178.85W	596.1	5.7	57	733	0.87	85	75	15	21	140	68	303	CMT
64	2/ 7/78	20.06S	178.25W	599.8	5.4	57	731	0.56	73	69	26	40	151	50	323	CMT
65	3/25/78	21.03S	178.84W	599.6	5.7	58	725	0.77	77	89	12	12	192	55	300	CMT
66	2/19/78	20.91S	178.75W	600.0	5.4	57	754	0.39	65	68	33	40	170	48	334	CMT
67	6/17/80	20.18S	178.44W	601.7	5.6	58	725	0.57	68	87	21	23	192	52	315	CMT
68	10/27/78	20.89S	178.67W	601.6	5.3	57	745	0.85	84	77	13	28	150	60	304	CMT
69	10/12/68	20.80S	178.70W	603.0	—	57	733	0.72	75	85	14	9	201	58	306	Bi
70	5/ 2/83	20.52S	178.67W	604.9	—	57	735	0.83	85	72	18	25	125	65	314	CMT
71	10/ 2/67	21.00S	178.80W	604.0	—	57	735	0.36	63	70	33	34	186	53	339	IM
72	4/24/79	20.83S	178.69W	604.2	6.0	57	744	0.65	85	58	32	23	158	66	350	CMT
73	2/13/80	21.10S	178.79W	605.0	5.4	58	763	0.63	77	67	26	34	152	56	328	CMT

Table 1. (*continued*)

	Event Information					Slab			Angle from down-dip			T Axis		P Axis		
	Date	Lat. (°)	Lon. (°)	Depth (km)	m_b	δ_s (°)	L (km)	κ	η_T (°)	η_B (°)	η_P (°)	δ (°)	θ (°)	δ (°)	θ (°)	Ref.
74	12/24/83	20.04S	178.42W	607.0	5.3	58	725	0.39	64	70	32	46	159	44	327	CMT
75	11/ 9/72	21.00S	179.00W	609.0	—	*57*	*752*	*0.63*	*72*	*85*	*20*	*33*	*168*	*51*	*312*	*Bi*
76	8/ 1/77	20.04S	178.21W	611.3	5.3	59	715	0.36	86	40	50	27	104	37	351	CMT
77	7/ 5/82	20.75S	178.88W	612.0	5.5	59	773	0.81	88	65	24	24	136	65	332	CMT
78	8/ 6/85	20.05S	178.36W	613.8	5.4	57	734	0.20	55	74	38	55	165	33	323	CMT
79	1/30/85	20.92S	179.12W	613.9	5.2	58	765	0.55	87	50	39	20	38	21	299	CMT
80	2/18/80	20.41S	178.50W	614.8	5.3	57	734	0.24	65	54	44	5	228	24	320	CMT
81	1/28/70	20.70S	178.80W	614.0	—	57	745	0.58	72	85	27	18	193	68	337	Bi
82	11/25/81	20.78S	179.01W	614.6	5.9	58	764	0.78	83	70	20	24	119	64	320	CMT
83	12/17/77	21.05S	178.79W	615.5	5.1	57	755	0.64	76	69	24	30	164	59	326	CMT
84	5/27/82	20.74S	178.96W	615.7	—	57	755	0.68	77	72	21	32	158	57	319	CMT
85	4/15/73	20.70S	178.80E	617.0	—	—	—	—	—	—	—	34	186	53	339	Bi
86	2/24/81	20.86S	178.62W	618.1	5.3	57	755	0.52	79	55	35	19	178	71	4	CMT
87	5/28/82	20.70S	178.84W	621.7	5.3	61	785	0.53	78	58	34	9	143	75	17	CMT
88	7/10/77	21.92S	179.25W	623.5	5.4	58	765	0.74	82	70	21	23	165	37	274	CMT
89	10/ 7/81	20.61S	178.80W	624.6	5.9	59	771	0.84	81	84	9	22	166	59	298	CMT
90	10/29/79	20.41S	178.62W	625.4	5.3	57	752	0.62	75	70	24	13	195	35	294	CMT
91	8/27/85	20.90S	179.06W	627.3	5.1	58	764	0.39	75	51	41	39	53	21	305	CMT
92	11/27/85	20.98S	179.16W	627.4	5.2	59	774	0.42	71	59	36	42	145	48	339	CMT
93	12/17/83	20.93S	178.94W	628.2	—	58	764	0.52	71	67	28	50	105	38	310	CMT
94	3/17/66	21.10S	179.20W	630.0	6.2	59	775	-0.19	38	74	54	24	300	64	132	ISO
95	9/16/80	20.62S	178.78W	631.3	5.3	63	801	0.52	83	51	39	31	124	50	350	CMT
96	9/ 5/84	21.01S	178.99W	633.3	5.3	61	785	0.82	83	75	16	35	91	51	302	CMT
97	6/25/77	21.32S	179.24W	633.7	5.4	63	802	0.64	72	81	18	44	108	45	269	CMT
98	10/12/67	21.10S	179.20W	636.0	—	61	781	0.52	86	48	40	32	109	43	341	IM
99	2/14/86	20.94S	179.03W	637.4	5.3	61	784	0.61	83	57	33	34	118	50	336	CMT
100	4/ 2/85	21.05S	179.22W	637.5	5.4	62	795	0.70	80	68	23	28	151	62	330	CMT
101	2/ 6/81	21.09S	178.93W	637.0	5.6	61	785	0.78	81	75	16	13	183	71	313	CMT
102	8/28/85	21.01S	179.01W	640.4	5.9	59	775	0.82	84	73	17	22	126	68	315	CMT
103	5/14/86	20.69S	178.79W	645.6	5.0	61	785	0.29	59	73	35	24	209	63	0	CMT
104	6/ 6/75	20.60S	179.10W	650.0	—	62	795	0.75	77	86	16	37	126	47	269	Bi
105	9/ 8/85	20.85S	179.07W	651.1	5.0	62	795	0.86	82	86	8	29	141	58	292	CMT
106	1/ 2/83	21.14S	178.32W	652.3	—	57	745	0.50	70	67	29	18	196	31	297	CMT
107	10/ 9/67	21.10S	179.30W	654.0	—	62	795	0.50	72	65	31	40	138	48	330	IM
108	12/14/77	21.10S	179.15W	657.6	5.6	63	805	0.66	85	59	31	22	100	53	337	CMT
109	1/26/72	20.20S	178.90W	660.0	—	62	795	0.60	74	86	28	34	153	56	335	Bi
110	1/ 9/85	20.70S	179.13W	660.4	5.3	63	802	0.22	56	71	39	53	46	24	279	CMT
111	11/30/85	20.95S	179.18W	662.1	4.9	59	775	0.37	60	81	30	9	233	74	354	CMT
112	1/10/77	20.72S	179.25W	666.2	5.5	61	835	0.68	80	67	25	21	28	36	282	CMT
113	11/28/79	20.77S	179.15W	678.0	5.4	62	824	0.58	71	76	23	46	101	42	298	CMT
114	10/22/85	20.16S	179.26W	684.5	5.0	61	835	0.30	59	74	35	59	105	30	302	CMT
115	10/10/84	20.16S	179.33W	691.3	5.6	59	842	0.49	66	78	26	46	49	33	276	CMT
116	6/17/77	19.88S	179.10W	693.9	5.7	59	842	0.68	83	62	28	18	61	42	314	CMT
T5	θ_s=282.7	$\overline{\delta_s}$=55														
1	7/28/80	22.12S	175.73W	75.1	5.4	33	62	0.77	78	88	11	65	133	22	283	CMT
2	3/23/71	22.90S	176.10W	77.0	—	43	112	0.92	87	80	10	44	108	44	268	Bi
3	8/20/65	22.90S	176.10W	79.0	—	43	113	0.87	86	74	15	50	93	40	263	ISO
4	8/25/81	22.76S	176.21W	108.0	5.8	43	109	-0.40	47	42	85	7	248	27	155	CMT
5	2/19/85	22.86S	176.81W	122.6	5.3	45	161	0.88	83	89	6	38	98	52	282	CMT
6	9/ 6/86	23.13S	176.97W	128.8	5.6	48	193	0.58	69	85	20	21	101	68	273	CMT
7	6/ 6/81	21.98S	176.10W	130.8	5.4	44	144	0.30	75	45	47	30	116	29	225	CMT
8	8/21/83	23.48S	177.19W	138.6	5.5	47	184	0.72	76	81	15	25	128	55	260	CMT
9	5/12/80	23.63S	177.19W	151.9	5.5	49	233	0.20	55	71	39	60	175	27	326	CMT
10	12/25/82	23.12S	177.24W	158.5	—	50	239	0.93	87	81	9	41	118	46	271	CMT
11	5/31/84	23.45S	177.41W	159.4	4.8	49	232	-0.08	68	24	80	62	115	9	8	CMT
12	4/13/80	23.47S	177.30W	166.2	6.7	48	193	0.64	79	65	27	31	101	51	325	CMT
13	1/27/86	23.74S	177.28W	169.4	5.1	48	224	0.85	84	76	15	27	61	42	303	CMT
14	3/25/86	21.86S	176.85W	189.0	5.1	50	244	0.77	80	78	14	48	115	42	300	CMT
15	1/ 4/82	23.05S	177.47W	190.5	6.0	51	255	0.81	83	73	17	31	115	58	312	CMT
16	12/17/85	21.46S	176.99W	201.3	5.1	50	245	0.74	84	63	26	34	107	49	324	CMT
17	1/25/85	22.87S	177.56W	202.3	5.5	52	283	0.76	80	75	17	44	134	46	308	CMT
18	8/ 5/79	22.72S	177.49W	229.2	6.4	52	284	0.83	86	71	19	32	124	57	315	CMT
19	11/10/81	23.22S	177.52W	232.7	5.2	54	315	0.91	84	86	6	29	85	59	291	CMT
20	4/29/79	22.71S	177.42W	236.9	5.4	55	335	0.34	61	74	33	4	83	59	347	CMT
21	6/25/83	22.04S	177.47W	273.5	5.5	55	345	0.69	78	69	23	22	84	52	322	CMT
22	4/28/69	22.40S	177.70W	296.0	—	61	383	-0.30	45	84	66	24	246	11	342	Ri
23	7/17/83	22.79S	178.13W	306.4	5.2	56	355	0.60	77	62	30	21	114	60	342	CMT
24	8/24/85	22.02S	177.84W	361.2	5.6	65	443	0.73	76	89	13	10	92	79	294	CMT
25	9/28/84	21.42S	177.98W	384.6	5.8	66	466	0.89	83	89	6	29	119	61	288	CMT

Table 1. (*continued*)

	Event Information					Slab			Angle from down-dip			T Axis		P Axis		
	Date	Lat. (°)	Lon. (°)	Depth (km)	m_b	δ_s (°)	L (km)	κ	η_T (°)	η_B (°)	η_P (°)	δ (°)	θ (°)	δ (°)	θ (°)	Ref.
26	10/26/85	21.89S	178.19W	396.1	5.0	70	484	0.90	83	84	8	23	140	62	282	CMT
27	3/28/86	22.94S	178.86W	398.4	5.4	71	506	0.68	89	56	33	19	101	52	345	CMT
28	9/ 8/79	22.89S	178.97W	448.9	5.1	64	575	0.53	69	75	26	16	206	45	314	CMT
29	12/25/85	21.56S	178.72W	461.8	5.6	64	573	0.29	81	39	51	30	138	44	15	CMT
30	9/30/78	23.01S	178.92W	467.3	5.4	64	585	0.81	80	89	9	30	143	56	291	CMT
31	1/14/79	22.53S	179.30W	488.0	5.2	65	625	-0.52	37	53	82	36	324	31	80	CMT
32	1/31/82	22.68S	179.24W	503.6	5.6	65	624	0.73	81	69	22	1	211	87	325	CMT
33	6/17/78	23.07S	179.59W	520.5	5.6	62	665	-0.43	28	78	64	52	334	10	231	CMT
34	2/11/87	22.70S	179.77W	524.1	5.1	62	685	0.19	60	59	44	47	43	43	211	CMT
35	2/ 8/81	23.60S	179.95E	535.7	5.3	56	724	0.91	85	89	3	31	61	53	279	CMT
36	6/16/86	21.90S	179.04W	564.8	6.1	62	675	0.93	86	82	8	27	135	62	300	CMT
37	3/27/79	21.61S	179.04W	574.5	5.3	61	695	-0.18	45	60	59	17	292	48	42	CMT
38	12/28/64	22.20S	179.60W	579.0	—	56	723	0.50	66	86	23	46	162	38	305	ISO
39	7/18/79	21.32S	178.80W	581.5	5.3	61	695	0.90	86	78	11	28	136	62	308	CMT
40	4/ 4/87	22.12S	179.63W	585.7	5.3	57	712	0.74	78	84	12	42	83	48	270	CMT
41	4/25/81	22.25S	179.41E	588.0	5.7	44	802	0.22	56	72	38	4	238	32	330	CMT
42	5/20/84	22.53S	179.40E	591.4	5.2	46	793	-0.57	20	84	69	26	276	64	102	CMT
43	12/26/80	22.21S	179.59W	591.6	5.5	55	751	0.80	86	67	22	22	42	67	241	CMT
44	11/25/79	21.99S	179.51W	593.4	5.4	55	732	0.60	70	85	19	49	63	39	266	CMT
45	4/10/83	22.13S	179.71W	593.6	5.3	55	745	0.50	89	44	45	29	65	21	322	CMT
46	9/25/84	22.27S	179.67W	594.9	5.1	55	753	-0.30	41	56	68	59	5	12	115	CMT
47	1/24/69	21.90S	179.50W	595.0	—	55	733	0.84	86	82	23	38	94	43	314	Bi
48	1/17/84	22.16S	179.77W	596.8	5.6	54	761	0.55	75	63	30	33	36	24	289	CMT
49	12/ 8/83	22.34S	179.72W	598.6	5.4	55	735	0.35	58	83	31	65	89	24	287	CMT
50	4/ 8/71	22.20S	179.50W	598.0	—	55	732	-0.41	29	82	62	64	341	6	92	Bi
51	7/ 2/86	21.95S	179.66W	598.3	5.5	55	734	0.84	86	71	18	38	96	47	309	CMT
52	7/17/86	21.81S	179.55W	599.0	4.8	57	711	0.58	73	75	22	37	160	35	283	CMT
53	12/ 2/81	21.82S	179.46W	599.7	5.6	54	761	0.91	88	75	14	37	94	48	304	CMT
54	4/20/87	21.67S	179.28W	600.6	5.3	56	721	0.75	78	87	12	42	71	44	280	CMT
55	7/ 8/79	22.19S	179.58W	600.4	5.5	55	745	0.97	89	81	8	32	79	52	295	CMT
56	10/23/77	21.68S	179.40W	600.9	5.0	57	713	0.32	77	47	45	45	98	29	334	CMT
57	7/10/77	21.82S	179.29W	603.3	5.3	55	735	0.68	72	89	16	48	135	40	292	CMT
58	5/26/86	21.72S	179.26W	603.4	5.9	55	731	0.85	84	77	13	3	7	43	274	CMT
59	9/25/77	21.83S	179.45W	607.3	5.4	56	724	0.47	83	49	41	38	80	28	325	CMT
60	8/17/78	22.17S	179.56W	607.5	5.6	55	755	0.72	76	86	13	10	151	65	264	CMT
61	2/20/86	22.01S	179.64W	607.0	5.6	55	745	0.69	79	69	23	45	109	42	313	CMT
62	1/15/80	22.21S	179.50W	607.9	5.5	54	760	0.67	75	76	19	20	86	70	255	CMT
63	1/30/80	21.76S	179.38W	609.4	5.4	55	750	0.72	85	62	28	39	95	41	320	CMT
64	9/ 1/87	21.81S	179.44W	612.5	—	55	744	0.75	78	76	17	45	87	41	298	CMT
65	12/21/78	21.82S	179.50W	612.8	5.6	55	743	0.65	76	70	24	48	108	40	311	CMT
66	9/24/87	21.69S	179.68W	613.9	—	54	761	0.59	69	86	21	55	85	34	274	CMT
67	4/22/84	21.83S	179.42W	616.6	5.7	55	733	0.26	55	88	33	59	163	25	303	CMT
68	2/19/80	21.92S	179.49W	617.2	5.4	55	743	0.24	53	86	35	69	130	21	294	CMT
69	9/10/62	21.30S	179.10W	618.0	—	55	730	0.45	66	72	30	10	87	60	341	IM
70	8/ 3/84	22.84S	178.97E	621.6	5.1	41	832	0.05	81	19	72	5	28	64	129	CMT
71	8/23/79	21.36S	179.40W	624.5	5.1	55	753	-0.31	32	85	58	69	215	6	322	CMT
72	9/12/68	21.60S	179.30W	632.0	—	55	752	0.36	64	82	36	9	107	66	0	Bi
73	11/16/84	21.46S	179.41W	633.3	5.2	55	745	0.58	70	78	22	54	114	34	272	CMT
74	11/24/80	22.54S	179.12E	636.3	5.3	41	868	0.66	73	80	19	7	164	56	264	CMT
75	2/22/80	21.56S	179.80E	652.3	5.3	42	814	0.73	78	73	19	50	56	25	293	CMT
76	2/10/69	22.70S	178.80W	670.0	—	55	735	0.19	54	82	38	35	207	45	343	Bi
77	3/ 9/78	20.89S	179.79W	679.5	5.2	41	871	-0.19	38	77	54	63	227	6	329	CMT
T6	θ_s=283.9	$\bar{\delta_s}$=56														
1	6/29/85	24.46S	176.64W	70.8	5.2	44	0	-0.34	31	89	59	74	260	14	114	CMT
2	1/20/70	25.80S	177.30W	80.0	—	46	63	0.46	69	80	35	53	159	37	331	Ri
3	2/ 6/79	25.41S	177.30W	82.6	5.4	46	60	0.78	78	84	12	24	65	51	302	CMT
4	4/29/82	24.73S	177.37W	114.0	—	51	120	0.69	89	56	33	38	119	46	335	CMT
5	8/12/67	24.70S	177.50W	134.0	6.5	51	143	-0.44	43	37	89	58	205	24	161	IM
6	1/ 4/85	26.07S	177.56W	138.6	5.3	51	125	0.18	64	51	48	56	156	34	348	CMT
7	8/15/68	23.90S	177.20W	186.0	—	52	173	-0.95	10	81	88	56	268	32	72	Bi
8	9/16/78	25.73S	177.95W	235.2	5.7	56	245	0.53	89	47	42	28	72	27	327	CMT
9	9/ 7/81	25.65S	178.01W	262.5	5.2	55	251	-0.42	41	52	76	17	266	5	358	CMT
10	2/22/75	24.98S	178.88W	333.0	6.6	58	373	0.29	86	82	69	32	79	51	115	Ri
11	1/19/84	23.63S	178.37W	335.7	5.9	58	355	0.56	71	73	25	50	104	38	262	CMT
12	2/ 7/84	25.68S	178.93W	355.1	5.4	58	375	0.65	75	75	20	30	36	38	279	CMT
13	7/21/73	24.83S	179.19W	373.0	6.1	58	424	-0.61	19	77	71	39	284	49	124	Ri
14	10/24/81	24.92S	179.01W	398.2	5.2	58	461	0.30	86	35	54	35	100	27	349	CMT
15	3/17/72	24.80S	179.60W	415.0	—	58	481	-0.31	34	82	59	50	344	8	243	Bi
16	8/ 8/77	23.81S	179.39W	445.1	5.2	60	521	0.00	86	5	86	6	18	33	112	CMT

Table 1. (*continued*)

	Event Information					Slab			Angle from down-dip			T Axis		P Axis		
	Date	Lat. (°)	Lon. (°)	Depth (km)	m_b	δ_s (°)	L (km)	κ	η_T (°)	η_B (°)	η_P (°)	δ (°)	θ (°)	δ (°)	θ (°)	Ref.
17	11/ 3/82	25.17S	179.72E	467.7	5.3	60	553	0.79	79	82	12	37	76	48	289	CMT
18	2/ 3/76	25.14S	179.70W	477.0	6.0	60	525	0.38	61	85	30	58	103	30	276	Ri
19	4/ 3/87	25.22S	179.77E	477.8	5.2	61	573	0.90	85	80	9	33	101	56	300	CMT
20	3/23/78	24.78S	179.90W	481.5	5.5	60	555	-0.11	42	75	51	61	19	26	227	CMT
21	7/ 3/79	23.86S	179.57W	494.3	5.1	60	565	0.61	71	79	21	6	138	82	281	CMT
22	3/21/84	22.91S	179.57W	499.5	5.1	60	562	0.39	62	77	30	46	44	42	243	CMT
23	9/20/84	24.33S	179.89W	505.1	5.3	61	584	0.65	83	61	29	35	97	48	236	CMT
24	10/13/85	25.16S	179.63E	506.7	5.0	61	581	0.74	78	77	16	39	88	51	260	CMT
25	1/29/79	24.66S	179.96E	509.4	5.5	62	595	0.79	80	79	14	36	86	54	261	CMT
26	11/12/84	24.95S	179.61E	512.2	5.1	62	593	0.44	70	63	34	47	92	34	315	CMT
27	9/16/83	23.95S	179.92W	517.3	5.9	62	594	0.55	71	72	26	39	55	36	289	CMT
28	2/21/85	23.95S	179.90W	521.4	5.0	62	604	0.74	78	77	16	13	75	62	320	CMT
29	4/ 5/81	25.04S	179.80E	521.4	5.3	62	595	0.09	60	51	52	57	98	21	332	CMT
30	11/22/81	24.00S	179.81W	527.8	5.4	54	632	0.85	86	73	17	27	50	61	254	CMT
31	6/27/83	23.71S	179.98W	528.9	—	60	613	0.81	88	66	23	29	81	46	316	CMT
32	7/26/81	23.86S	179.99E	531.1	5.2	58	625	0.38	61	78	30	58	76	28	290	CMT
33	9/26/84	23.92S	179.91E	534.0	5.0	60	615	0.13	59	56	48	58	79	19	317	CMT
34	3/23/74	23.90S	179.80W	535.0	—	62	605	0.08	57	83	51	60	90	19	324	Ri
35	12/ 3/86	24.13S	179.96W	539.1	5.2	58	623	0.65	74	76	20	45	81	39	296	CMT
36	12/28/73	23.90S	179.90W	539.0	—	60	614	0.21	54	83	36	60	60	24	284	Ri
37	12/26/86	24.23S	179.61E	539.7	4.9	58	623	0.33	59	78	32	53	48	26	277	CMT
38	11/18/86	24.07S	179.82E	540.9	5.3	60	611	0.25	57	73	37	61	90	25	300	CMT
39	8/20/87	24.16S	178.89E	542.3	—	50	681	0.81	87	67	22	33	58	33	303	CMT
40	11/20/71	23.40S	179.90W	543.0	—	58	620	0.38	64	82	34	55	74	35	245	Bi
41	3/14/85	23.70S	179.98W	545.9	5.0	58	625	-0.03	59	43	61	62	88	11	337	CMT
42	2/ 7/82	23.34S	179.13E	546.3	—	50	682	-0.02	59	43	61	3	73	55	168	CMT
43	7/17/78	23.64S	179.99W	547.4	5.4	58	622	0.24	67	52	46	50	65	17	313	CMT
44	10/ 7/63	23.60S	180.00E	548.0	—	58	625	0.52	67	81	25	51	73	33	284	ISO
45	2/20/86	23.47S	179.83W	552.1	5.2	54	635	0.84	81	84	9	19	62	56	301	CMT
46	4/28/81	23.72S	179.98E	553.3	6.0	58	625	0.51	69	73	27	47	63	31	291	CMT
47	3/12/84	23.29S	179.87E	555.9	5.5	58	623	0.44	68	67	32	53	93	31	309	CMT
48	2/ 9/80	23.91S	179.43E	556.3	5.3	50	675	0.36	76	48	44	4	41	82	158	CMT
49	1/17/65	24.60S	178.40E	557.0	—	50	695	-0.32	43	53	71	34	228	54	69	ISO
50	7/17/80	23.60S	179.03E	558.1	5.0	51	705	0.12	84	23	67	19	30	55	149	CMT
51	5/18/78	22.96S	179.98W	558.1	5.3	54	635	0.63	74	75	21	17	81	58	323	CMT
52	8/ 6/86	23.66S	179.75E	558.4	5.0	54	630	0.19	59	63	43	66	116	21	321	CMT
53	5/12/82	24.55S	179.08E	559.8	5.6	50	664	0.58	87	51	38	42	105	36	334	CMT
54	9/ 8/63	23.60S	180.00E	559.0	—	54	634	0.41	61	89	27	62	75	27	278	ISO
55	6/20/83	23.53S	179.05E	561.9	5.6	50	683	0.17	72	38	55	21	12	66	160	CMT
56	9/17/82	23.45S	179.95W	561.5	5.9	51	644	0.67	73	86	17	53	81	34	284	CMT
57	8/ 2/84	23.46S	179.95W	561.7	5.4	51	640	0.72	78	75	18	0	213	68	303	CMT
58	7/20/79	23.35S	179.94W	566.4	5.4	51	644	0.33	79	44	48	49	98	24	336	CMT
59	9/29/85	23.22S	179.17E	566.2	4.9	50	692	0.18	75	37	56	8	49	66	157	CMT
60	3/29/79	24.05S	178.55E	568.6	5.4	52	740	-0.48	31	65	71	31	253	56	104	CMT
61	8/26/84	23.57S	179.07E	571.8	6.0	52	725	0.87	82	88	7	22	176	50	295	CMT
62	9/14/86	23.30S	178.99E	571.3	5.2	52	714	0.01	62	41	61	2	238	62	144	CMT
63	7/10/85	23.60S	178.81E	572.2	5.1	52	730	0.26	68	52	45	11	215	78	57	CMT
64	7/18/84	23.79S	179.80W	575.3	5.5	54	635	0.78	89	62	27	4	20	27	288	CMT
65	12/28/84	23.54S	179.11E	576.7	5.3	51	705	0.80	79	88	10	6	203	53	301	CMT
66	9/11/81	23.32S	179.16E	580.6	5.2	51	703	0.01	63	41	62	2	236	63	141	CMT
67	7/23/87	23.35S	179.73E	594.9	—	50	674	-0.02	52	57	54	25	345	65	169	CMT
68	12/22/82	23.59S	179.41E	597.0	—	50	695	0.66	84	59	30	4	28	22	297	CMT
69	12/22/86	22.66S	179.25E	618.1	5.2	52	724	0.31	59	77	33	19	220	34	323	CMT
T7	θ_s=285.1	$\overline{\delta_s}$=55														
1	1/28/78	25.92S	177.30W	97.6	6.0	56	82	0.32	72	50	43	51	105	29	334	CMT
2	4/12/71	26.70S	177.10W	101.0	—	47	54	0.04	67	79	65	65	102	10	349	Ri
3	7/27/86	25.90S	177.49W	109.2	5.8	57	94	0.38	86	39	49	29	106	35	353	CMT
4	8/ 1/68	26.60S	177.50W	123.0	5.6	57	103	-0.14	46	69	57	44	210	3	305	Ri
5	2/ 7/83	26.54S	177.80W	157.4	—	59	145	0.86	86	72	17	33	91	50	311	CMT
6	11/23/78	26.18S	177.69W	190.5	5.5	56	183	-0.02	44	87	45	37	224	38	350	CMT
7	7/ 4/63	26.30S	177.80W	190.0	—	58	175	0.31	65	60	39	1	71	39	339	IS
8	7/21/64	26.00S	177.90W	200.0	—	54	194	0.73	78	75	19	47	107	42	308	ISO
9	8/31/87	26.74S	178.65W	315.5	—	56	315	0.26	76	41	51	20	102	35	357	CMT
10	4/19/82	25.97S	178.81W	357.9	—	59	374	0.62	77	66	27	43	97	43	249	CMT
11	8/17/81	25.45S	179.06W	396.9	5.5	60	445	0.76	80	74	17	38	94	51	258	CMT
12	5/ 7/77	25.75S	179.95E	462.3	5.4	52	534	0.72	88	59	30	23	52	28	309	CMT
13	8/23/84	27.18S	179.73W	462.9	5.1	55	504	-0.21	60	28	86	27	208	31	100	CMT
14	5/27/81	25.36S	179.85E	499.6	5.3	49	594	0.62	84	57	33	34	95	48	233	CMT
15	8/ 2/85	24.41S	179.53E	523.4	5.1	49	592	0.50	68	73	27	18	94	60	330	CMT

Table 1. (*continued*)

	Event Information					Slab			Angle from down-dip			T Axis		P Axis		
	Date	Lat. (°)	Lon. (°)	Depth (km)	m_b	δ_s (°)	L (km)	κ	η_T (°)	η_B (°)	η_P (°)	δ (°)	θ (°)	δ (°)	θ (°)	Ref.
16	2/16/83	25.33S	179.62E	526.6	5.4	49	605	0.75	82	69	21	47	88	36	307	CMT
17	3/30/72	25.70S	179.40W	532.0	—	52	541	0.63	74	80	25	46	61	28	295	Ri
18	2/15/71	25.20S	178.40E	589.0	—	54	722	0.79	84	81	18	6	177	73	289	Bi
19	4/18/78	25.21S	178.41E	598.4	5.6	55	734	0.68	69	78	23	52	76	33	292	CMT
20	5/ 3/87	25.16S	178.35E	630.6	5.2	56	763	0.57	75	84	15	19	100	69	305	CMT
21	2/19/85	25.79S	178.17E	649.3	5.1	64	803	0.34	63	80	28	24	207	61	349	CMT
22	7/ 7/87	25.52S	177.84E	655.3	—	64	802	0.56	71	74	24	28	180	60	339	CMT
T8	θ_s=288.0	$\overline{\delta_s}$=57														
1	2/25/87	27.96S	177.08W	74.6	5.0	38	68	-0.35	31	82	59	69	305	16	83	CMT
2	1/24/76	28.60S	177.60W	78.0	5.8	43	90	-0.42	27	58	66	48	327	8	61	Ri
3	3/ 7/72	28.20S	178.30W	192.0	6.1	54	223	0.08	54	27	40	12	245	42	348	Ri
4	9/19/77	27.80S	177.99W	202.8	5.1	52	215	0.22	61	59	43	9	98	47	358	CMT
5	10/20/85	28.97S	178.91W	262.0	5.3	58	284	0.15	71	39	56	13	111	36	11	CMT
6	5/11/72	27.70S	178.90W	355.0	—	54	394	0.46	65	79	27	59	129	31	309	Ri
7	3/ 5/86	26.51S	178.18E	634.9	5.1	61	793	0.05	57	54	52	58	73	14	320	CMT
8	2/27/80	27.43S	178.30E	637.4	5.5	61	795	-0.02	74	20	77	28	178	13	81	CMT
T9	θ_s=293.5	$\overline{\delta_s}$=66														
1	10/19/84	30.54S	178.38W	92.0	5.5	46	92	0.95	88	83	6	45	112	45	284	CMT
2	6/25/84	30.90S	178.89W	139.3	5.2	64	160	0.74	76	87	13	38	100	52	286	CMT
3	10/ 5/82	30.23S	178.06W	162.6	5.5	60	155	0.19	87	27	62	27	79	10	344	CMT
4	6/26/81	30.27S	178.99W	163.8	5.7	66	176	0.87	83	84	8	29	102	59	302	CMT
5	7/ 4/81	30.33S	178.90W	184.6	5.3	65	196	0.73	85	62	27	19	96	52	341	CMT
6	1/26/83	30.36S	179.43W	224.1	6.1	63	235	0.41	66	68	32	38	177	52	354	CMT
7	4/20/87	30.47S	179.02W	231.3	5.2	66	255	0.71	77	76	19	36	98	49	310	CMT
8	3/ 6/84	29.00S	179.12W	298.5	5.2	72	326	0.24	62	61	41	11	280	52	25	CMT
9	9/28/81	29.31S	179.23W	309.1	5.9	72	317	0.54	79	57	34	28	103	45	341	CMT
10	1/31/81	30.55S	179.52W	319.3	5.1	72	346	0.02	51	63	49	21	284	47	39	CMT
11	3/28/72	30.70S	178.80W	337.0	5.6	72	326	0.30	75	37	42	1	87	42	356	Ri
12	2/13/78	30.02S	179.29W	340.1	5.3	70	366	0.37	77	47	44	7	114	47	17	CMT
13	1/20/68	29.90S	179.50W	349.0	6.0	67	373	0.65	81	85	36	11	87	76	115	IM
14	5/ 3/81	30.05S	179.80W	440.6	5.0	60	445	0.29	57	81	33	9	258	76	29	CMT
15	4/ 2/85	30.45S	179.02E	539.4	5.0	62	595	0.46	75	57	36	17	203	72	41	CMT
T10	θ_s=300.1	$\overline{\delta_s}$=70														
1	8/19/81	33.47S	179.66E	211.8	5.1	69	256	0.82	81	83	10	2	231	65	325	CMT
2	8/ 5/64	32.20S	179.80E	216.0	—	69	256	-0.60	22	75	72	58	254	32	74	ISO
3	9/13/86	31.65S	179.97W	231.0	5.8	70	275	0.42	69	63	34	2	282	55	15	CMT
4	9/ 4/67	31.40S	179.40W	231.0	6.2	70	263	-0.28	22	83	49	55	263	32	241	IM
5	3/ 5/82	31.57S	179.73E	232.1	—	70	286	0.81	88	66	23	21	122	59	351	CMT
6	7/23/84	30.36S	179.65W	336.7	5.3	72	386	0.32	75	47	46	3	120	45	27	CMT
7	11/21/77	31.45S	179.89W	341.1	5.2	72	386	0.00	55	53	54	17	290	38	33	CMT
8	3/14/77	31.01S	179.94E	352.4	5.0	71	396	0.62	81	60	30	9	96	52	355	CMT
9	1/ 7/82	31.52S	179.30E	425.3	—	69	475	0.43	76	53	39	6	104	46	7	CMT
10	12/ 5/86	31.20S	179.76E	432.8	5.4	66	482	0.98	86	88	3	15	81	68	309	CMT
11	11/ 8/79	32.31S	179.20E	455.1	5.7	66	485	0.32	60	74	33	12	262	55	10	CMT

Events in each slice are in ascending order of focal depths. δ_s is slab plunge. L is the subducted slab length measured from the slab trace at 50 km depth to the event. κ is down-dip stress index. η_T, η_B and η_P are angles between the down-dip direction and T-, B- and P-axes, respectively. In each slice, θ_s is slice azimuth and $\overline{\delta_s}$ is the average slab plunge of all events deeper than 100 km.

The references are: ALK – Astiz et al., 1988; CMT – Dziewonski and Woodhouse, 1983, Giardini, 1984, and Dziewonski *et al.*, 1983a-c, 1984a-c, 1985a-d, 1986a-c, 1987a-g, and 1988a-f; Bi – Billington, 1978; BJ – Berckhemer and Jacob, 1968; Cn – Chandra, 1971; FK – Fujita and Kanamori, 1981; HIM – works by Honda and Masatsuka [1952] and Honda *et al.* [1967] as compiled by Isacks and Molnar, 1971; Hi – Hirasawa, 1966; Ic – Ichikawa, 1966; IM – Isacks and Molnar, 1971; ISO – Isacks *et al.*, 1969; KS – Katsumata and Sykes, 1969; OI – Oike, 1971; RA – Ritsema, 1965; Ri – Richtrer, 1979; SM – Stauder and Maulchin, 1976; ST – Sengupta and Toksöz, 1977.